Oil palm (*Elaeis guineensis*) plantation on tropical peatland in South East Asia: photosynthetic response to soil drainage level for mitigation of soil carbon emissions

***Jon McCalmont[1,7], Lip Khoon Kho[2,6], Yit Arn Teh[3], Melanie Chocholek[4], Elisa Rumpang[2], Lucy Rowland[1], Mohd Hadi Akbar Basri[1,5], Tim Hill[1]**

[1] College of Life and Environmental Science, University of Exeter, Streatham Campus, Rennes Drive. Exeter, EX4 4RJ. UK

[2] Peat Ecosystem and Biodiversity Unit, Biology and Sustainability Research Division, Malaysian Palm Oil Board, 6, Persiaran Institusi, Bandar Baru Bangi, 43000 Kajang, Selangor, Malaysia

[3] School of Natural and Environmental Science, Newcastle University, Drummond Building, Newcastle-upon-Tyne, NE1 7RU UK

[4] Dept. Earth and Environmental Science, University of St. Andrews, Irvine Building, North Street, St. Andrews, KY16 9AL. UK.

[5]Dept. of Crop Science, Faculty of Agriculture, Universiti Putra Malaysia, 43400 Serdang, Selangor, Malaysia

[6]Economic Planning Unit, Sarawak Chief Minister's Dept., 93502, Kuching, Sarawak, Malaysia

[7]School of Biological Sciences, University of Aberdeen, King's College, Aberdeen, AB24 3FX

***Corresponding author (jon.mccalmont@abdn.ac.uk)**

Abstract

While existing moratoria in Indonesia and Malaysia should preclude continued large-scale expansion of palm oil production into new areas of South-East Asian tropical peatland, existing plantations in the region remain a globally significant source of atmospheric carbon due to drainage driven decomposition of peatland soils. Previous studies have made clear the direct link between drainage depth and peat carbon decomposition and significant reductions in the emission rate of CO_2 can be made by raising water tables nearer to the soil surface. However, the impact of such changes on palm fruit yield is not well understood and will be a critical consideration for plantation managers. Here we take advantage of very high frequency, long-term monitoring of canopy-scale carbon exchange at a mature oil palm plantation in Malaysian Borneo to investigate the relationship between drainage level and photosynthetic uptake and consider the confounding effects of light quality and atmospheric vapour pressure deficit. Canopy modelling from our dataset demonstrated that palms were exerting significantly greater stomatal control at deeper water table depths (WTD) and the optimum WTD for photosynthesis was found to be between 0.3 and 0.4 m below the soil surface. Raising WTD to this level, from the industry typical drainage level of 0.6 m, could increase photosynthetic uptake by 3.6% and reduce soil surface emission of CO_2 by 11%. Our study site further showed that despite being poorly drained compared to other planting blocks at the same plantation, monthly fruit bunch yield was, on average, 14% greater. While these results are encouraging, and at least suggest that raising WTD closer to the soil surface to reduce emissions is unlikely to produce significant yield penalties, our results are limited to a single study site and more work is urgently needed to confirm these results at other plantations.

Keywords:

Oil palm, eddy covariance, tropical peatland, CO_2 emission, photosynthetic uptake, drainage level

1 Introduction

Southeast Asian peatlands cover an area of around 250,000 km^2 and store around 69 Pg of carbon, around 5% of the global soil carbon pool (Page *et al.*, 2011, Scharlemann *et al.*, 2014, Gumbricht et al., 2017). However, the need for economic development has seen very large-scale agro-industrial development on these peatlands over the last three decades through the establishment of monoculture plantations across the region. Satisfaction of the global demand for agricultural commodities has seen around 8 Mha of peatland in Malaysia and Indonesia converted to monoculture plantation with the majority of this being for palm oil production (Miettinen *et al.*, 2016; Cheng *et al.*, 2018; Gaveau *et al.*, 2018). As a result, more than 2.5 Pg of CO_2 was released to the atmosphere between 1990 and 2015 as a result of carbon oxidation driven by forest clearance and peat soil drainage (Miettinen *et al.*, 2017). Current government and industry moratoria (Busch *et al.*, 2015; Padfield *et al.*, 2016; Chen *et al.*, 2019), if adhered to, should mean there are no new large-scale peatland conversions from forest to oil palm for these two largest global producers of palm oil; however, existing plantations in the region need to be better managed to minimise peat loss and limit CO_2 emission rates.

Studies (Hooijer *et al.*, 2010; Couwenberg & Hooijer, 2013; Marwanto &Agus, 2013; Husnain *et al.*, 2014; Ishikura *et al.*, 2018), including our own (McCalmont *et al.*, 2021), have shown that peat decomposition, and resulting CO_2 emission, is directly related to soil water drainage level and adjusting water table depth (WTD) through strategic management is one of the few environmental drivers of decomposition that is readily available to manipulation by plantation managers. The latest Round Table on Sustainable Palm Oil (RSPO) Best Management Practice guidelines (RSPO 2018) recommend maintaining WTD between 0.3 and 0.6 m below the peat surface (as measured by in-situ piezometers), closer to the surface than in their earlier advice (RSPO 2013) which had suggested 0.4 m as the lower limit. This revised recommended lower limit of 0.3 m is slightly at odds with the stated concern in the earlier manual that the top 0.5 m of the soil profile was the area of concentration for palm 'feeder' roots which must not be waterlogged. A synthesis dataset presented by Prananto *et al.* (2020), showed that typical commercial drainage levels are at the deeper end of this scale, the mean drainage depth across 78 tropical peatland plantations was 0.57 m, with oil palm specifically (56 sites) at 0.55 m. These WTD levels are at the shallower end of industry standard recommendations; the Water Management Guidelines manual developed by the Department of Irrigation and Drainage in Sarawak, Malaysian Borneo, recommend draining peatland to a minimum of 0.6 m, and up to 0.75 m, for oil palm plantations (DID, 2001).

Drainage to these depths, and beyond, results in substantial soil CO_2 emission; work by Hooijer *et al.* (2010) suggested that emissions increase by around 9 Mg CO_2 ha^{-1} yr^{-1} for each 0.1 m of drainage below the soil surface. Our own results later showed that this relationship is not linear and benefits in reduced soil emissions may be much greater if WTD is moved back towards the upper soil layers (McCalmont *et al.*, 2021); we showed that peat surface emissions of CO_2 at the shallower end of the RSPO range (0.3 m) could be around 20% lower than at the deeper end (0.6 m).

Less well known is the potential impact on fresh fruit bunch (FFB) yield that shallower WTD may result in, a vital consideration for plantation managers. One manipulation experiment, presented as a conference paper (Ginting &Darlan, 2016), reported that raising WTD from 0.6-0.7 m to 0.4-0.6 m reduced soil CO_2 emission by 18% and increased FFB yield by 3%, a finding supporting earlier results by Othman *et al.* (2011), who found WTD between 0.35 m and 0.45 m to be optimal for FFB yield, similar to Winarna *et al.* (2017) who showed yields to be highest at 0.35-0.50 m.

In a free draining soil such as peat, WTD has a direct impact on plant available water in the rooting zone above; Adhi *et al.* (2021) suggested maintaining WTD between 0.4 and 0.6 m, optimising FFB yield and minimizing fire risk by ensuring soil layers above the water table do not dry out. Soil water content (SWC) in the rooting zone can be reduced by as much as 255% when WTD are below 0.7 m (Ginting &Darlan, 2016), an important consideration as *Elaeis guineensis* show evidence of early stomatal closure under water limitation; even in a free draining sandy soil, palms failed to reduce extractable water fraction below 40% (Dufrêne *et al.*, 1993). Shallower WTD ensures soil surface layers are kept wetter, due to capillary action, helping to minimize soil water deficit and facilitating upward mobility of nutrients (Henson *et al.*, 2008). Henson *et al.* (2008) state that, generally, sites with shallower WTD give higher yields though there must be sufficient depth of unsaturated soil in the upper layer, due to a danger that water logging of the roots might result in plant nitrogen (and possibly sulphur) deficiency. However, they discuss earlier work using lysimeters (Henson & Mohd, 2004) which found that palms established in peat could be extremely resilient to WTD being maintained very near the soil surface. Following a brief period of depressed stomatal conductance and photosynthesis the palms appeared to recover, likely due to an observed proliferation of fine roots at the soil surface produced in response to the water logging. This resilience to waterlogging was also seen in the field experiments of Peralta-Lobo *et al.* (1985) and Marwanto and Hendri (2021), who reported that excessive drainage during periods of high rainfall resulted in nutrient leaching and negative impacts on FFB yield and showed that palms could be resilient, or even benefit, from periods of inundation though this resilience may only last for a short time before restrictions on root respiration begin to impair water and nutrient uptake (Woittiez *et al.*, 2017). It is possible that substantial lateral flow of ground water, due to operation of water control gates in drainage channels, may promote aeration of the soil water and reduce anaerobic conditions, even where WTD is within the rooting zone (Henson *et al.*, 2008). One study (Henson & Chang, 2000), monitoring a mature oil palm plantation where, on average, around a third of the root biomass (and occasionally more than 50%) was below the WTD, found that FFB production did indeed remain high (> 36 Mg ha^{-1} yr^{-1}).

Quantifying, and modelling, the impact of WTD specifically on photosynthetic uptake (GPP) at the canopy level is not straightforward due to multiple confounding parameters; particularly temporal variability in atmospheric vapour pressure deficit (VPD, the difference between the storage capacity for water vapour in the air and the actual vapour content), and the quality of the incoming light. Studies have shown that the fraction of incoming light which is diffuse has a significant bearing on canopy-scale CO_2 assimilation (Hollinger *et al.*, 1994; Gu *et al.*, 2002; Cheng *et al.*, 2015; Wang *et al.*, 2018); an emergent property of canopy structure where diffuse light penetrates further into the lower canopy and there is less light saturation in the upper canopy (Knohl & Baldocchi, 2008). This enhancement was found to be greater in a tropical, broadleaf forest, compared to boreal and temperate broadleaf, (Alton et al., 2007) with the suggestion that this was due to the tropical site having a higher leaf area index (5.5, similar to a mature oil palm canopy (Henson & Dolmat, 2003)), though Knohl and Baldocchi (2008) showed the effect was consistent even when comparing single and multi-layer canopy structures. They reported an interaction between diffuse fraction and atmospheric humidity, as conditions with a high diffuse fraction of incoming radiation are typically associated with cloudy conditions when VPD impacts on stomatal conductance are reduced. Zhang *et al.* (2020) also found a positive relationship between diffuse light and photosynthesis and similarly found an interaction with relative humidity, suggesting that the beneficial effect decreased as VPD increased beyond 1 kPa.

Atmospheric vapour pressure deficit is the primary driver of water movement (and contained nutrients) through plant vascular systems and, where VPD generates leaf water potentials substantially exceeding soil water availability, most plants must protect themselves from embolism through reducing stomatal conductance. Isohydric species, such as *Elaeis guineensis* (Grossiord *et al.*, 2017; Waite *et al.*, 2019), try to maintain a constant leaf water potential, irrespective of VPD, using sensitive stomatal control but are susceptible to limitations in soil water availability. Waite *et al.* (2019) compared P_{50} values (the xylem pressures found at 50% loss of hydraulic conductivity) for *Elaeis guineensis* fronds under different soil water conditions and found that palms on well-drained soils showed P_{50} values 25% more negative when compared to riparian sites (-2.07 vs -1.65 MPa). They reported that these relatively high P_{50} values are similar to other tree (and tree-like) species from the moist tropics and agreed with earlier studies (Rowland *et al.*, 2015; Santiago *et al.*, 2018; Oliveira *et al.*, 2019) suggesting that these species may be particularly vulnerable to soil water deficits. However, despite stomatal closure in *Elaeis guineensis* (indicated by a reduction in evapotranspiration) beginning when VPD exceeds 1 kPa (Kallarackal *et al.*, 2004), significant impacts on CO_2 uptake are not seen until VPD reaches around 1.8 kPa (Dufrene & Saugier, 1993; Kallarackal *et al.*, 2004) with palm productivity remaining resilient to relatively high levels of VPD provided there is sufficient water available in the soil profile (Smith, 1989).

Soil water availability, and therefore the capacity to supply atmospheric demand, follows directly from the hydrological management of the plantation (within the seasonal limitations of rainfall) with drainage levels, and consequently water table depth, being directly under the control of plantation managers. Our study investigates the relationship between water table depth and photosynthetic uptake of CO_2 at a mature *Elaeis guineensis* plantation at the canopy scale, using high frequency monitoring of gas exchange by eddy covariance. We address the question of whether WTD may be brought closer to the soil surface than the typical 0.6 m without negatively impacting photosynthetic uptake (and subsequent fruit yields) and whether there may be an optimum mean WTD for yield. Finally, we use results from our previous study to estimate the corresponding impacts on CO_2 emission that may result from manipulating WTD to optimise yields.

2 Methods

2.1 Site description

Eddy covariance (EC) and meteorological data used in this study were collected over a three-year period (April 2017 to August 2020) at a commercially managed, mature oil palm plantation (Sebungan) on peatland in Sarawak, northern Malaysian Borneo (3° 9.965′ N, 113° 21.198′ E). The plantation was originally established into cleared peat swamp forest during 2007/2008, with the palms being around 10 years old when EC monitoring began. More details of the site can be found in McCalmont *et al.* (2021), where we report detailed CO_2 fluxes and the overall carbon balance (see also Cook *et al.* (2018) and Manning *et al.* (2019) for site information and additional flux monitoring). The site was originally established into deep peat (up to 8 m depth) in 2007 at a planting density of ~160 palms ha^{-1} with the existing forest logged, cleared, and drained by a regular network of drainage channels. The eddy covariance tower, and peak contribution to the flux integration, is situated within a specific plantation block (07/25), an area of 42.96 ha, located centrally within the wider Sebungan plantation which covers a total of 907 ha and 43 planting blocks, all consistently managed under standard industry practice.

2.2 Instrumentation

Full details of instrumentation, data processing and quality control can be found in McCalmont *et al.* (2021). Briefly, a LI-COR closed path eddy covariance system (LI-7200/7550 infra-red gas analyser, LI-COR Environmental, and R3-50 sonic anemometer, Gill Instruments Ltd) was mounted at the top of an 18 m tower (around 12 m above canopy height). Incoming global solar radiation (**Rg**, W m^{-2}) was also monitored at the top of the tower, using a 4-channel net radiometer (CNR4, Kipp and Zonen), with incoming diffuse radiation (**Rd**, W

m^{-2}) measured using a sunshine pyranometer (SPN1, Delta-T). Photosynthetically active radiation (**PPFD**, µmol m^{-2} s^{-1}) was measured using a quantum sensor (LI-190SL-50, LI-COR Environmental). Canopy profile sensors: air temperature (**Tair**, degC), relative humidity (**Rh**, %) and CO_2 concentration (**Ca**, ppm) (HMP155A, GMP343, Vaisala Corporation), were installed at 1 m, 6 m, and 18 m above the ground to monitor, and correct for, canopy storage of energy, CO_2 and water vapour (Montagnani *et al*., 2018). Soil temperature (**Tsoil**, degC) and moisture (**SWC**, m^3 m^{-3}) were recorded at two replicate locations (~15 m from the tower base) and two depths (0.04 m and 0.2 m), (Steven's Hydraprobe, Steven's Water Monitoring Inc.) and combined with soil heat flux plates ((HFP01SC, Hukseflux), installed at 0.08 m at the same location, to monitor soil energy storage. Water table depth (**WTD**, m) monitored within a 0.05 m diameter porous plastic pipe inserted to a depth of 2.5 m (PX709GW submersible pressure transducer, Omega Engineering Inc.). Rainfall was recorded at the top of the tower with a tipping bucket rain gauge (TR-525M, Texas Electronics). Wind components and CO_2 concentrations were measured at 10 Hz and processed to half-hour mean flux rates (µmol CO_2 m^{-2} s^{-1}), meteorological data were recorded at one-minute intervals and again processed to half-hourly mean rates (or sums for rainfall).

2.3 Dataset compilation:

Raw CO_2 concentrations and associated wind turbulence parameters were collected at 10 Hz and processed into 30-min average net ecosystem exchange CO_2 flux rates (**NEE**, µmol CO_2 m^{-2} s^{-1}) using EddyPro software (v6.2.2 LI-COR Environmental). Full details of data collection, quality control and correction for profile storage are reported in McCalmont et al. (2021).

Following data quality control and flux processing, gross primary productivity (**GPP**, gross photosynthetic uptake of CO_2 into the canopy, µmol CO_2 m^{-2} s^{-1}) was partitioned from **NEE**, (µmol CO_2 m^{-2} s^{-1}) following the nighttime-based air temperature response (Lloyd & Taylor, 1994; Reichstein *et al*., 2005) of ecosystem respiration (**Reco**, µmol CO_2 m^{-2} s^{-1}); the residual of NEE being GPP (i.e., GPP = Reco-NEE). This approach can result in half hours with negative values of GPP, in this case there were 488/22280 negative GPP values which were removed from the analysis. Only original measured data points (not gap filled) were used and filtered to daytime only (defined as periods where PPFD was above 50 µmol m^{-2} s^{-1}). A dimensionless light quality indicator (**diffFrac**) was added representing the fraction of diffuse light within the global incoming solar radiation, calculated as **Rd/Rg**. Only periods where data were complete for all parameters (GPP, PPFD, diffFrac, SWC, Tair, Tsoil, VPD (vapour pressure deficit, kPa), WTD) were retained, this resulted in a total of 14,022 half hour data points to go forward into the analyses. Data compilation and analyses were carried out using R (version R-4.04, R Core Team 2021)

2.4 Comparison of GPP measured within WTD bins

Data were binned into 0.1 m WTD increments and the distribution of GPP was compared between them using the Wilcoxon Rank Sum test (to accommodate non-normal distribution and unequal sample sizes between bins). Data were transformed to equal variance (using a reciprocal transformation) between bins prior to testing.

2.5 Relative importance of measured parameters

Factor analysis was used to demonstrate the relationship between the measured parameters and GPP. First, co-linearity was investigated using a simple correlation matrix (based on Pearson's coefficient); subsequently the high levels of co-linearity, which were seen between multiple parameters, were accommodated by using principal component regression. Measured parameters were combined into seven principal components (PCs), following data centring and scaling, and the correlation between PCs and GPP was investigated, again using Pearson's correlation coefficient. Next, the seven PCs were used as independent variables in a multiple linear regression to GPP, and the model bootstrapped 1000 times, using the R package "relaimpo" (Gromping, 2006), to produce an estimate of the relative contribution to model explanatory power for each of the individual PCs. Loadings within each of them, and the cumulative contribution to the overall regression model, were used to indicate parameters which were most influential on GPP.

2.6 Light response modelling

Using non-linear, least squares regression (NLS), a rectangular hyperbolic function (Eq.1) was fitted between PPFD and GPP to estimate light use efficiency (LUE, the initial slope of the curve [α]) and maximum assimilation of CO_2 (the asymptote, A_{max} [β]).

For an initial overview, the model was first fitted to all data within each WTD bin to produce an estimate of overall LUE and A_{max} for individual WTD bins. To investigate the impact of light quality (diffuse fraction) and vapour pressure deficit, the data were further binned into diffFrac and VPD bins (four quartiles each) and the model again fitted to individual

WTD bins within these. The resulting parameter estimates (LUE and A_{max}) were then used with PPFD fixed to the mean measured daytime value recorded over the study period (824.7 μmol m^{-2} s^{-1}) to model GPP and compare across WTD bins, i.e., for a fixed intensity of light, how does WTD impact GPP across a range of diffFrac or VPD conditions? Uncertainty estimation for predicted GPP (upper and lower bounds of the 95% confidence intervals) was carried out through Monte Carlo simulation using the 'propagate' package in R (Spiess, 2018)

Finally, functional coefficients were added to Eq.1 to modify the impact of PPFD on GPP based on the combination of light quality and VPD (Eq.2). The VPD modification incorporates the exponential coefficient (k) of Lasslop *et al.* (2010), which limits the increase in GPP due to increasing PPFD at higher VPD levels (in our case beyond a threshold of 1.8 kPa as reported in Dufrene and Saugier (1993)). In addition to VPD, a further linear coefficient (c) was incorporated which increases GPP as incoming light becomes more diffuse. The updated model (Eq. 2) was first fitted across all data to derive a universal value for c which was then fixed, and the model re-fitted within WTD bins to estimate α and β and k specific to those bins. Finally, to provide a scenario comparison across WTD bins, model parameters specific to each WTD bin (along with the universal value for c) were used to estimate GPP across the entire dataset (at the half hour resolution). This resulted in an estimate of daytime GPP flux rate (μmol CO_2 m^{-2} s^{-1}) at a half-hour timestep across the three-year period fixed to each of the six WTD bins, i.e., what would the half-hourly GPP be if WTD remained at each 0.1 m WTD increment throughout the study period? Uncertainty estimation for the predictions was again carried out through Monte Carlo simulation as above.

To convert from mean daytime flux rate (μmol CO_2 m^{-2} s^{-1}) to an annual GPP sum (Mg CO_2 ha^{-1} yr^{-1}), the mean modelled GPP flux rate (μmol CO_2 m^{-2} s^{-1}) estimated for each WTD bin scenario across the three year dataset was multiplied by the mean number of seconds annually that PPFD was above 50 μmol m^{-2} s^{-1} (i.e., daytime, when photosynthesis would be occurring) to produce an annual sum and then unit converted to Mg CO_2 ha^{-1}. Mean measured daytime GPP flux rate (across the study period) was similarly converted to an annual sum. This allowed modelled annual GPP fixed to individual WTD bins to be compared as a delta to the measured value.

Equation 1:

$$GPP = \frac{\alpha.\ \beta \cdot PPFD}{\alpha.PPFD + \beta}$$

Where:

GPP = *gross primary productivity (photosynthetic uptake, µmol CO_2 m^{-2} s^{-1})*

PPFD = *photosynthetic photon flux density (photosynthetically active radiation, µmol m^{-2} s^{-1})*

α = *light use efficiency (LUE, µmol CO_2 $umol^{-1}$ PPFD)*

β = *maximum assimilation (*A_{max}*, µmol CO_2 m^{-2} s^{-1})*

Equation 2:

$$GPP = \frac{\alpha.\,(\beta \cdot ((1 - c \cdot (1 - diffFrac)) \cdot \exp\,(-k \cdot (VPD - VPD_0\,)) \cdot PPFD}{\alpha.PPFD + (\beta \cdot ((1 - c \cdot (1 - diffFrac)) \cdot \exp\,(-k \cdot (VPD - VPD_0\,))}$$

$$When\, VPD < VPD_0\!: \ \exp\big(-k \cdot (VPD - VPD_0)\big) = 1$$

Where:

diffFrac = *diffuse fraction of incoming solar radiation*

VPD = *vapour pressure deficit (kPa)*

VPD_0 = *baseline threshold for the impact of VPD on limiting* A_{max} *(1.8 kPa)*

c and **k** = *derived coefficients*

2.7 'Big Leaf' canopy modelling

To investigate the impact of WTD on canopy functioning, two further parameters were considered. The stomatal slope parameter (G1), representing the slope of the relationship between canopy surface conductance (Gsw) and GPP (normalised to atmospheric CO_2 concentration (Ca) and relative humidity (Rh)), Eq.3, (Ball *et al.*, 1987) and the atmospheric decoupling coefficient (Ω), Eq.4, (Jarvis & McNaughton, 1986), ranging from zero to 1, with decreasing values indicating increased stomatal control in the canopy. Canopy modelling was carried out using the 'Bigleaf' package in R (Knauer *et al.*, 2018). G1 was estimated by fitting Eq.3 within each WTD bin separately (using NLS regression), with the intercept of the slope (G0) fixed to zero, while Ω was calculated at the half hour timestep across the entire dataset (using Eq.4), with the mean and standard errors subsequently calculated for each WTD bin. The impact of increasing WTD on both parameters was investigated through testing the significance of the slope of an ordinary least squares (OLS) regression.

In addition to the data filtering described above, only periods where the canopy surface could be assumed to be dry were included in the canopy modelling; data points were retained only where the last recorded rainfall (>0.02mm) was at least 24 hours earlier. Following this additional data filtering there were 4895 half hourly data points remaining where all necessary parameters for the canopy modelling were available.

The derivation of parameters (and associated references) underlying Eq.3 and Eq.4 (to estimate G1 and Ω) from the eddy covariance measurements can be found in supplementary materials: aerodynamic conductance (G_{ah}) for heat and canopy surface conductance for water vapour (G_{sw}) were calculated using Eq.S1 to Eq.S4, while canopy surface conditions for Tair, VPD and CO_2 concentrations were derived from measurements made at the EC sensor heights using bulk transfer functions (Eq.S5 to Eq.S8).

Equation 3:

$$G_{sw} = G0 + G1 \cdot \frac{(GPP \ \cdot Rh)}{Ca_{surf}}$$

Where:

G_{sw} = *canopy conductance for water vapour (m s^{-1})*

G0 = *intercept of the slope (fixed at zero)*

G1 = *stomatal slope parameter*

GPP = *gross photosynthetic uptake of CO2 (µmol m^{-2} s^{-1})*

Rh = *relative humidity (%)*

Ca_{surf} = *atmospheric CO_2 concentration at canopy surface (µmol mol^{-1})*

Equation 4:

$$\Omega = \frac{{}^{s}/_{\gamma} + 1}{{}^{s}/_{\gamma} + 1 + {}^{G_{ah}}/_{G_{sw}}}$$

Where:

Ω	=	*atmospheric decoupling coefficient*
s	=	*slope of saturation vapour pressure curve (kPa degC^{-1})*
γ	=	*psychrometric constant (kPa degC^{-1})*
$\mathbf{G_{ah}}$	=	*atmospheric conductance for heat (m s^{-1})*
$\mathbf{G_{sw}}$	=	*canopy conductance for water vapour (m s^{-1})*

2.8 Monthly yield, FFB vs GPP

To investigate the relationship between measured photosynthetic uptake (GPP) and fresh fruit bunch (FFB) yield, an ordinary least square regression was carried out between monthly summed GPP (gap filled GPP data summed to monthly totals of carbon (Mg CO_2-C ha^{-1} mth^{-1})) and the carbon content of FFB dry biomass (Mg CO_2-C ha^{-1} mth^{-1}). Carbon gain into FFB was assumed to be equal to the monthly harvest offtake and calculated from the block specific monthly yield data (supplied by the plantation manager) using the mean moisture (72%) and carbon (43.57%) contents of FFB collected at the study site and reported in Lewis *et al.* (2020).

2.9 Inter-block comparison of yield and WTD

Finally, a comparison was made, for monthly yield and water table depth, between the specific study block where the Eddy Covariance system was located, (07/25), and the 42 other blocks within the Sebungan plantation. WTD depth is recorded once a month across the plantation from piezometers (one per block), installed by the plantation management. For the purposes of comparing WTD across blocks, data from the plantation WTD monitoring is used for 07/25 (rather than data from the Eddy Covariance WTD sensor). Data from these piezometers was available for two years, 2019 and 2020.

Specific yields (Mg FFB ha^{-1} mth^{-1}) are commercially sensitive data so, for a comparison between our study block and the other planting blocks across the site, we report only the relative difference (%) between individual planting blocks and the plantation mean, also limited to years 2019 and 2020

3 Results

3.1 Comparison of GPP measured within WTD bins

Water table depth (WTD) for the study block (07/25) within the retained dataset ranged between 0 and 0.59 m below the soil surface, with a mean of 0.27 ± 0.001 m (± S.E.M.). Binning in 0.1 m increments therefore resulted in six WTD bins: [0,0.1], [0.1,0.2], [0.2,0.3], [0.3,0.4], [0.4,0.5], [0.5,0.6].

There were no significant differences in GPP flux rates measured within the first four WTD bins (spanning 0 to 0.4 m WTD), with a mean uptake rate across these at 27.0 ± 0.27 μmol CO_2 m^{-2} s^{-1}. GPP flux rates in the WTD bins ranging between 0.1 and 0.4 m were all significantly higher than the two deepest bins (covering 0.4 to 0.6 m), however, the shallowest WTD bin (0 to 0.1 m) recorded a mean GPP rate (26.42 ± 0.3 μmol CO_2 m^{-2} s^{-1}) which was not significantly different to the deepest WTD bin (0.5 to 0.6 m) at 25.63 ± 0.5 μmol CO_2 m^{-2} s^{-1}). See Fig. 1 and Supplementary table S1. for mean and median GPP rates for individual WTD bins and Supplementary table S5. for means of VPD, diffFrac and PPFD measured within each WTD bin.

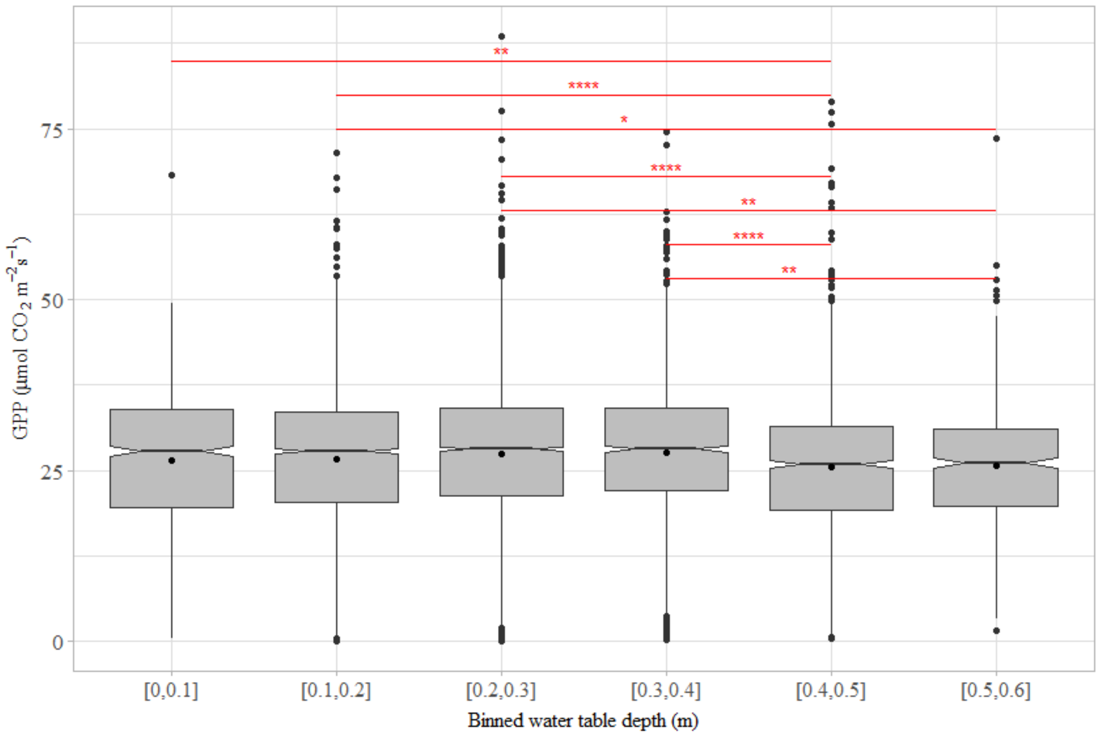

Figure 1: *Boxplot comparison of GPP data distribution within water table depth bins. Points within boxes indicate the mean flux rate for the WTD bin, notches are centred on the median and show the 95% confidence interval (1.5 * IQR/n). Red over-bars and asterisks indicate significant differences resulting from pairwise Wilcoxon Rank Sum testing (significance code: p < 0.0001****, <0.001 ***, <0.01 **, <0.05 *). Values for mean and median flux rates, and number of data points per WTD bin, are given in Table S1. in supplementary materials*

3.2 Inter-block yield and WTD comparison

The study block, 07/25, was typically poorly drained compared to the other plantation blocks (Fig. 2a). Mean WTD at 07/25, across the two years of the plantation piezometer data, was 0.268 ± 0.021 m below the soil surface (remarkably close to a mean of 0.267 ± 0.001 m measured at the EC tower in the same block), compared to a mean of 0.535 ± 0.005 m across all blocks.

Monthly yields from 07/25 were typically greater than the plantation mean, averaging 14.71 ± 6.68 % higher across the two years of the yield data (Fig.2b).

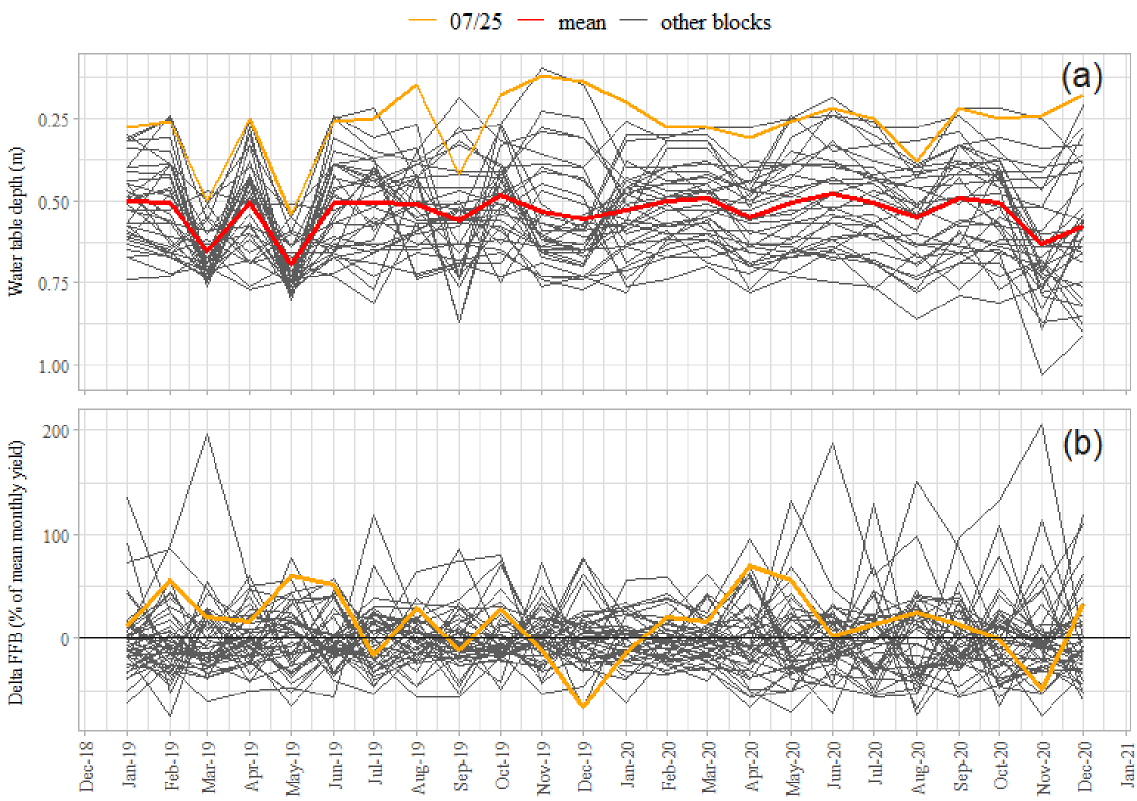

Figure 2: *Plot (a) shows water table depth below the soil surface (recorded once monthly from in-situ piezometers) for the 43 individual planting blocks within the Sebungan plantation (note Y-axis scale is reversed, data points nearer the top are closer to the soil surface). The orange line highlights the eddy covariance study block (07/25), the red line shows the mean for each month across all blocks. Plot (b) shows the percentage difference to the mean yield (at Y = 0) for each month for each of the 43 planting blocks, orange again highlighting 07/25.*

3.3 *Factor analysis*

Table 1 shows the relative contribution of individual PCs to the multiple regression model (in order of importance), their respective loadings and the percentage contribution to each PC from them. The model fit was highly significant ($f_{(4,14014)} = 1532$, $p<0.0001$) and explained around 43% of the variation in GPP, with all PCs being shown to be highly significant in the fit ($p<0.0001$). The three most important components (PC6, PC2 and PC1) contributed 74% to the total model power (see Table 1) and were loaded primarily by light and its quality (PC6, 29% of total model power)), soil moisture status (PC2, 25% of total model power) and air temperature and VPD (PC1, 20% of total model power). A correlation matrix between individual parameters (Fig.S1) and a summary of the regression model can be seen in supplementary materials, along with correlation between GPP and all 7 PCs (Table S2.).

Table 1 *Principal components (PCs) and their loadings in order of importance to a multiple regression with GPP. Vertical data columns show percentage contribution of each loading to the individual PC, bottom row shows cumulative contribution (%) to total model explanatory power (43.3%).*

PC6		PC2		PC1		PC3		PC5		PC7		PC4	
Variable	Loading (%)	Variable	Loading (%)	Variable	Loading (%)	Variable	Loading (%)	Variable	Loading (%)	Variable	Loading (%)	Variable	Loading (%)
PPFD	51.70	SWC	33.60	Tair	25.71	PPFD	18.27	Tsoil	41.82	Tair	53.61	WTD	55.06
diffFrac	33.70	WTD	26.35	VPD	24.66	diffFrac	17.88	diffFrac	23.45	VPD	44.11	SWC	42.85
Tsoil	10.17	Tsoil	16.41	diffFrac	17.39	Tsoil	17.24	VPD	17.87	Tsoil	1.29	diffFrac	0.90
VPD	3.42	PPFD	15.86	PPFD	13.93	SWC	15.69	Tair	9.39	SWC	0.58	Tair	0.78
Tair	0.67	diffFrac	6.67	Tsoil	12.92	WTD	12.48	SWC	5.74	WTD	0.35	VPD	0.23
WTD	0.28	VPD	1.07	WTD	3.91	Tair	9.80	WTD	1.56	PPFD	0.04	Tsoil	0.14
SWC	0.06	Tair	0.04	SWC	1.48	VPD	8.64	PPFD	0.17	diffFrac	0.01	PPFD	0.04
28.7		**54.1**		**73.9**		**86.3**		**95.1**		**99.8**		**100**	

Cumulative percentage contribution to model power

3.4 *Light response modelling*

The modelled light response curve (Eq. 1), fitted across all data, resulted in estimates for LUE, the initial slope (α), at 0.15 ± 0.002 µmol CO_2 (µmol PPFD)$^{-1}$ and A_{max}, the asymptote (β), at 39.22 ± 0.21 µmol CO_2 m^{-2} s^{-1} (± standard error of the estimate) with both parameter estimates being highly significant ($P<0.0001$). Figure 3 shows a comparison of Eq.1 fitted within each of the WTD bins across all light quality and VPD data. LUE was similar across all WTD, with a mean of 0.15 ± 0.007 µmol CO_2 (µmol PPFD)$^{-1}$. A_{max} was more variable between WTD bins and typically lower with deeper drainage, reflected in the separation between the individual curves as PPFD increases. The greatest A_{max} (42.63 ± 0.9 µmol CO_2 m^{-2} s^{-1}) occurred in the 0 to 0.1 m WTD bin and the lowest (35.39 ± 0.6 µmol CO_2 m^{-2} s^{-1}) in the 0.4 to 0.5 m WTD bin.

The relationship between modelled GPP uptake rate (µmol CO_2 m^{-2} s^{-1}) within WTD bins for a fixed light intensity varied significantly when considered within light quality and VPD quartiles (Fig.4). Overall, there were clear trends to higher GPP with more diffuse light conditions and lower vapour pressure deficits. For light quality the highest GPP rate was predicted under the 4th quartile of diffuse light (diffuse fraction of incoming radiation at 0.9 to 1) where GPP peaked under the 0.3 to 0.4 m WTD bin at 34.08 [32.6, 35.1] µmol CO_2 m^{-2} s^{-1} (*values in square brackets show the 95% confidence intervals of the predicted GPP*). Under the vapour pressure deficit scenarios, the highest GPP was predicted under the 1st quartile of VPD (0 to 0.59 kPa), again within the 0.3 to 0.4 m WTD bin at 33.41 [31.7, 34.6] µmol CO_2 m^{-2} s^{-1} (Fig.4, tables S3 & S4).

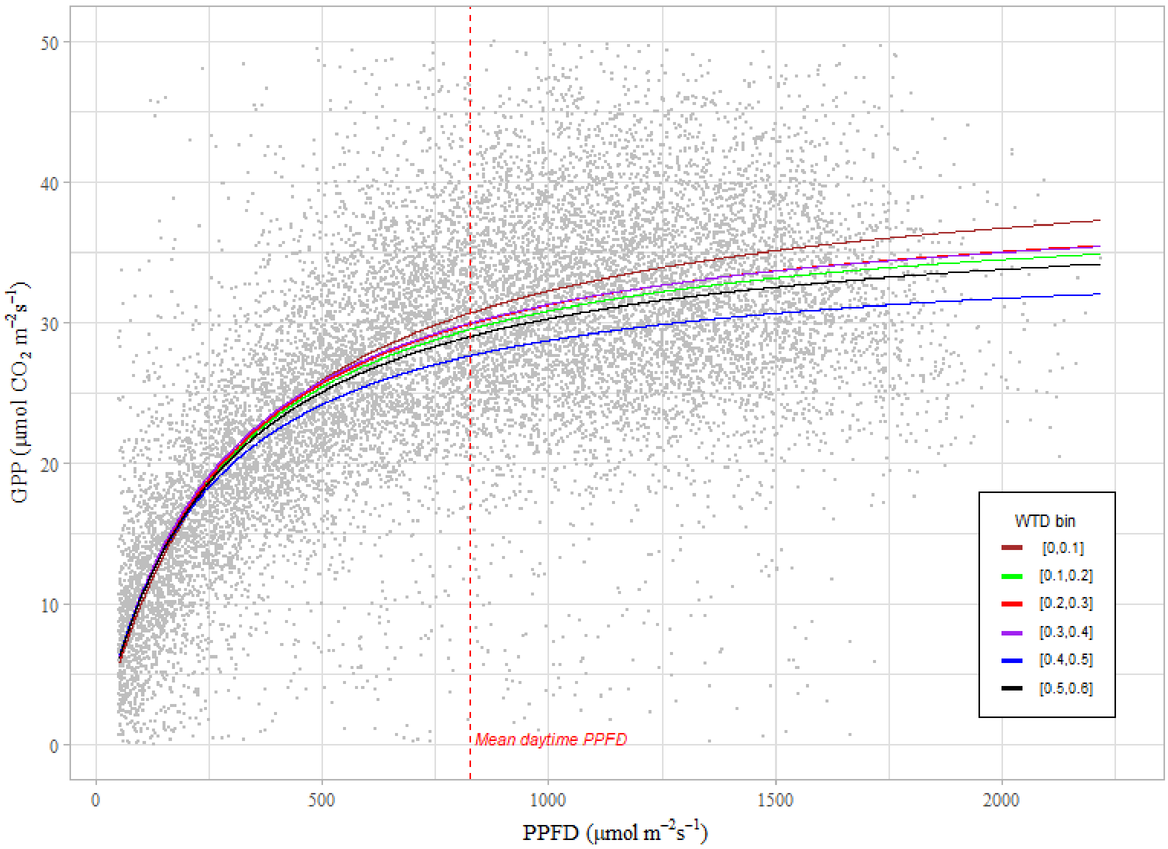

Figure 3: *Light response curves between photosynthetically active radiation (PPFD) and photosynthetic uptake of CO_2 (GPP), fitted within water table depth (WTD) bins at 0.1 m increments. Dashed red line shows the mean annual daytime PPFD over the three-year dataset*

Following incorporation of the effects of diffuse fraction and VPD into the light response model (Eq.2) there remained no clear linear trend seen between increasing WTD and LUE or A_{max} (Fig.5). The highest LUE (0.109 ± 0.003 µmol CO_2 µmol $PPFD^{-1}$) was found for WTD between 0.3 and 0.4 m depth while greatest A_{max} (60.37 ± 0.61 µmol CO_2 m^{-2} s^{-1}) was seen for WTD between 0.2 and 0.3 m (Fig. 5a & 5b). Figure 5c shows the subsequent predictions of mean GPP for each WTD bin with error bars showing the 95% confidence interval (CI), values with CI ranges overlapping are not significantly different to each other.

GPP for WTD between 0.4 and 0.5 m (25.89 [25.27, 26.47] µmol CO_2 m^{-2} s^{-1}) was significantly lower than for WTD both between 0.2 and 0.3 m (27.04 [26.71, 27.37] µmol CO_2 m^{-2} s^{-1}) and between 0.3 and 0.4 m (27.36 [26.94, 27.76] µmol CO_2 m^{-2} s^{-1}). GPP in the 0.3 to 0.4 m WTD bin was also significantly higher than for the 0.1 to 0.2 m WTD bin (26.46 [26.07, 26.84]). See Table 2 for GPP rates estimated for all individual WTD bins).

The x axis (y=0) in Fig.5c indicates the mean measured annual GPP (176.3 ± 0.6 Mg CO_2 ha^{-1} yr^{-1}), data points show how much the modelled annual GPP within each WTD bin deviates from measured GPP. Resulting from the combination of LUE and A_{max} shown in Fig.5a and 5b, WTD in the two bins covering 0.2 and 0.4 m showed the greatest predicted GPP (mean 178.43 [175.98,180.82] Mg CO_2 ha^{-1} yr^{-1}), though of the two bins only WTD bin 0.3 to 0.4 m (179.47 [176.75, 182.10] Mg CO_2-C ha^{-1} yr^{-1}) was seen to be significantly greater than measured GPP. All other WTD depths predicted GPP lower than measured GPP, though only WTD bins [0.1,0.2] and [0.4,0.5] were seen to be significantly different, likely due to the large error bars around values for [0,0.1] and [0.5,0.6].

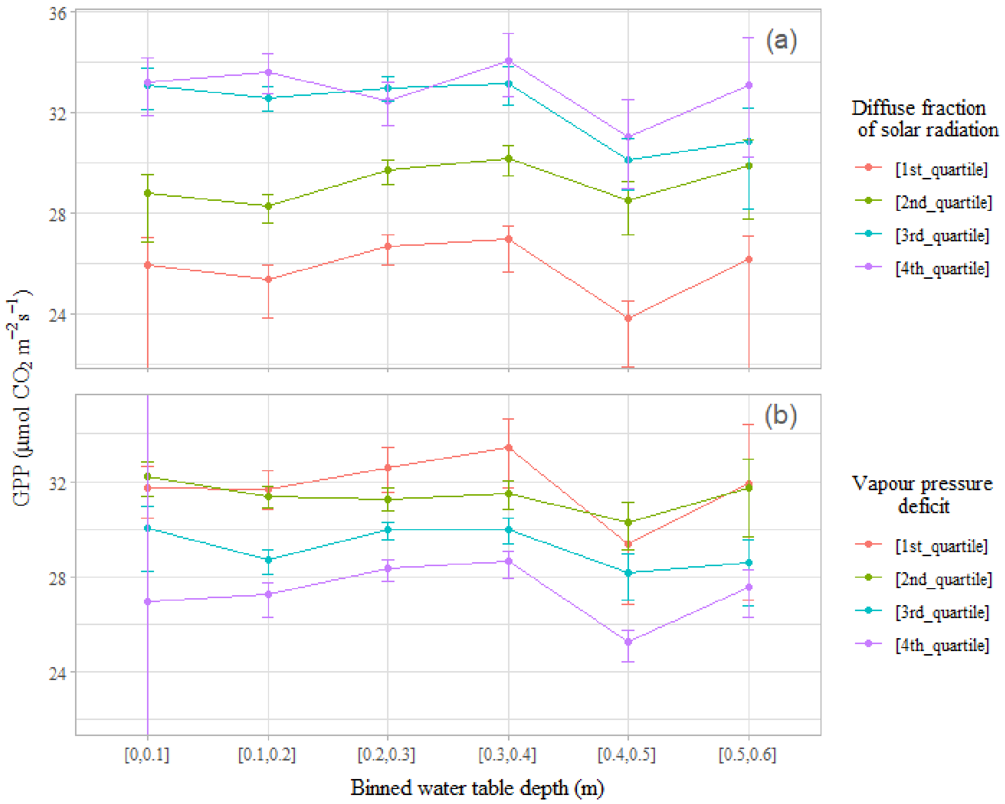

Figure 4: *Impact of WTD on modelled GPP (unmodified light response model, Eq. 1) under individual quartiles of diffuse fraction of solar radiation (a) and vapour pressure deficit (b). Error bars show 95% confidence intervals. Light response curves for all individual data bins can be seen in supplementary materials, Fig.S2. with complete tables of individual data bin results given in Table S3 (diffFrac) and Table S4 (VPD)*

Table 2: *Comparison across WTD bins of parameter estimates (LUE and A_{max}) and model predictions for GPP flux rate, mean annual sum and potential change (delta GPP) from annual mean GPP measured across all three study years. ± values show the standard error of the model parameter fit. Values in square brackets show the 95% confidence intervals for predicted GPP. n() shows the number of half-hour data points which were available for parameter estimation within each WTD bin.*

WTD bin [m]	LUE (α) [μmol CO_2 μmol^{-1} PPFD]	Amax (β) [μmol CO_2 m^{-2} s^{-1}]	k	GPP estimated [μmol CO_2 m^{-2} s^{-1}]	GPP estimated [Mg CO_2 ha^{-1} yr^{-1}]	delta GPP [Mg CO_2 ha^{-1} yr^{-1}]	n()
[0.0,0.1]	**0.10** ± 0.003	**58.36** ± 1.25	**1.42** ± 1.05	**25.89** [24.57,27.31]	**169.84** [161.19,179.18]	**-6.49** [-15.14,2.85]	**1000**
[0.1,0.2]	**0.11** ± 0.002	**57.84** ± 0.63	**0.32** ± 0.10	**26.46** [26.07,26.84]	**173.56** [171.00,176.07]	**-2.77** [-5.33,-0.26]	**3812**
[0.2,0.3]	**0.10** ± 0.002	**60.37** ± 0.61	**0.23** ± 0.06	**27.04** [26.71,27.37]	**177.39** [175.21,179.53]	**1.06** ['-1.12,3.20]	**4860**
[0.3,0.4]	**0.11** ± 0.003	**59.49** ± 0.78	**0.01** ± 0.04	**27.36** [26.94,27.76]	**179.47** [176.75,182.10]	**3.14** [0.42,5.77]	**2350**
[0.4,0.5]	**0.10** ± 0.004	**56.64** ± 1.20	**0.29** ± 0.05	**25.89** [25.27,26.47]	**169.81** [165.76,173.63]	**-6.52** [-10.57,-2.70]	**1543**
[0.5,0.6]	**0.11** ± 0.006	**56.52** ± 1.80	**0.11** ± 0.10	**26.38** [25.41,27.28]	**173.06** [166.67,178.95]	**-3.27** [-9.66,2.62]	**457**

± S.E. of the model fit. [95% confidence intervals]

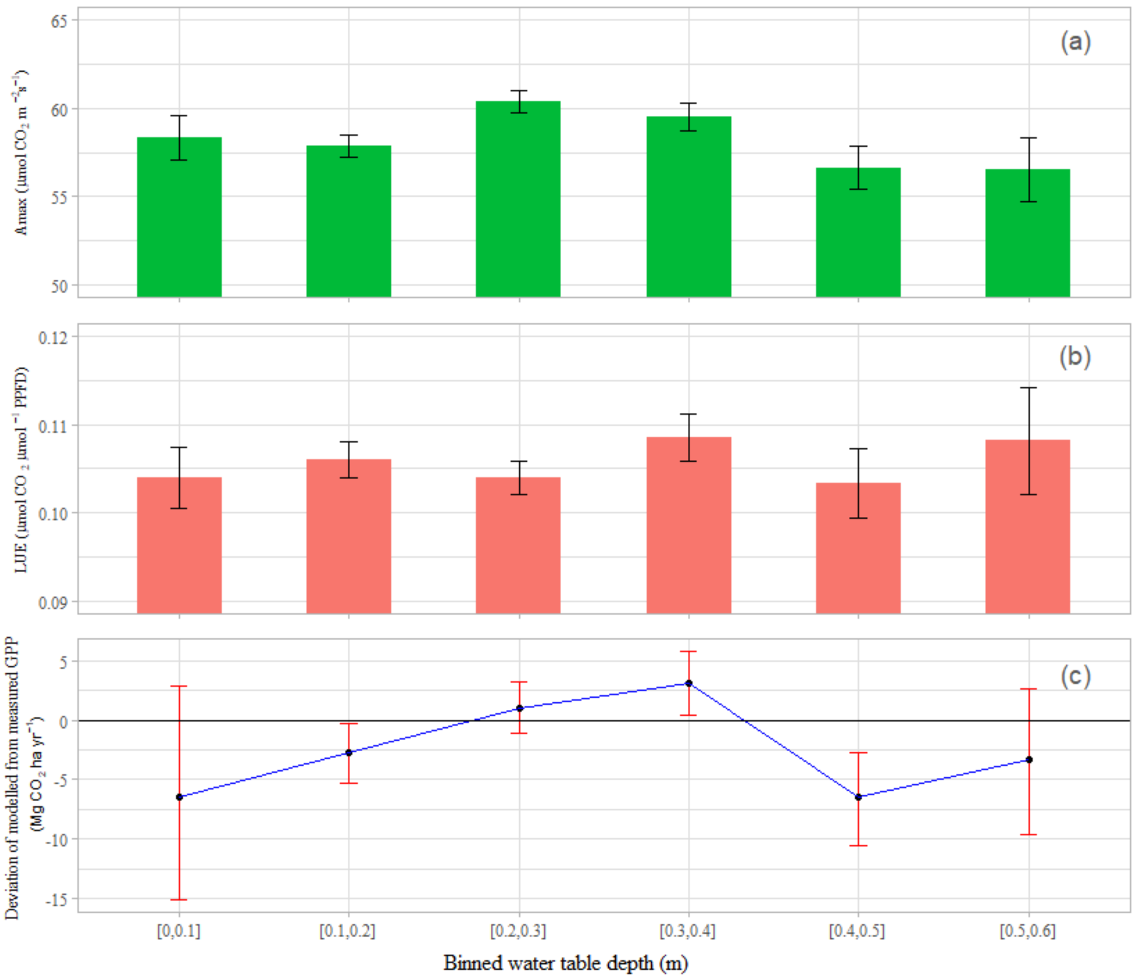

Figure 5: *Impact of WTD on maximum assimilation (A_{max}) of CO_2 (a), light use efficiency (b) and modelled change in GPP due to water table depth (WTD) relative to the measured annual mean (c). Error bars in (a) and (b) show the standard error of the model parameter estimate. Error bars in (c) show 95% CI of the predicted value, error bars crossing zero show values not significantly different to the measured mean annual GPP. See Table 2 for values of LUE, A_{max} and modelled GPP for each of the WTD bins, along with number of data points available to the model fitting.*

3.5 Canopy modelling

There was a clear and significant reduction in the G1 and Ω parameters with increasing WTD (G1: $f_{(1,4)} = 39.64$, $p<0.01$, $R^2 = 0.88$, Ω: $f_{(1,4)} = 102$, $p<0.001$, $R^2 = 0.95$; Fig 6). For each increase in 0.1 m WTD bin, G1 decreased by 6% while Ω decreased by 3%. Large standard errors seen in the 0 to 0.1 m WTD bin estimates for G1 and Ω and are likely the result of limited data availability within that bin (Table S6).

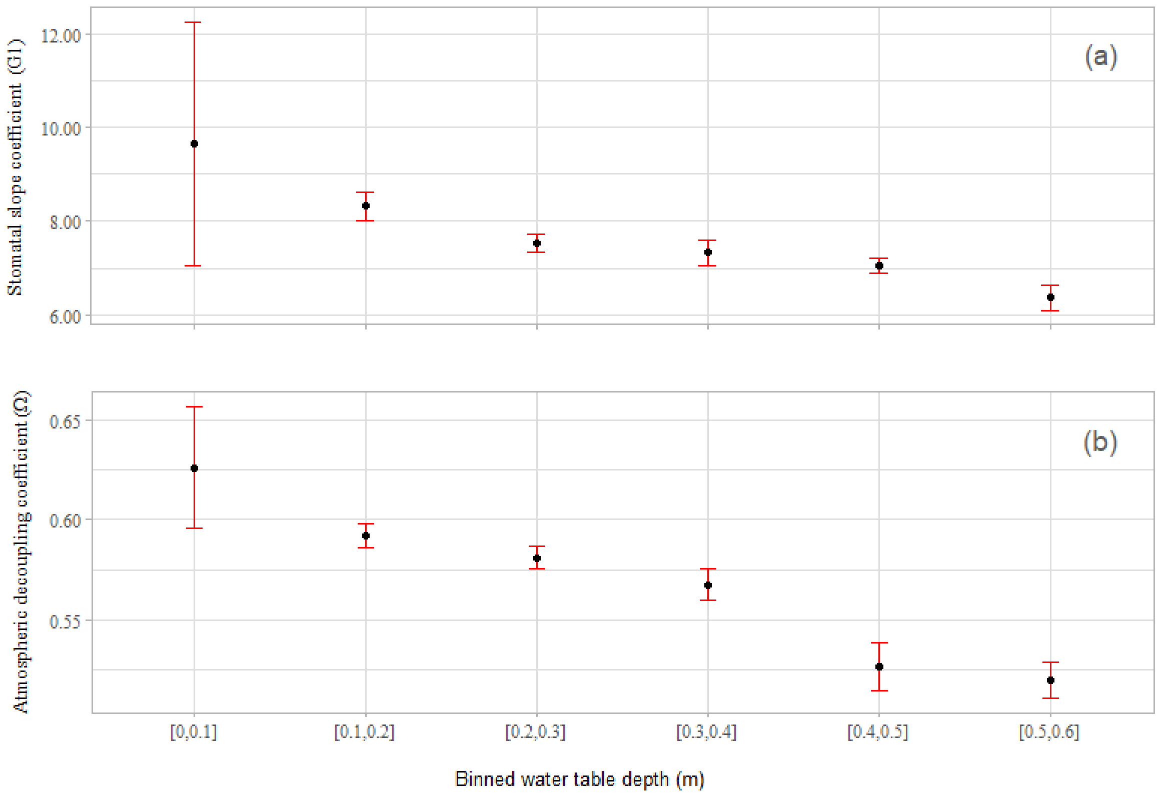

Figure 6: *Stomatal slope (a) and atmospheric decoupling (b) coefficients within water table depth bins. Points in (a) show the G1 parameter estimate derived within each WTD, with error bars showing ± the standard error of the estimation. Points in (b) show the mean of the half hourly decoupling coefficients within each WTD bin with error bars showing ± the standard error of this mean.*

3.6 Monthly yield, FFB vs GPP, block vs plantation

The relationship between the carbon contents of monthly fresh fruit bunch (FFB) yield and GPP for the years 2019/20 was highly significant ($f_{(1,16)} = 9.52$, $p < 0.01$, $R^2 = 0.37$) with the slope of the regression line suggesting that FFB represented around 11% of concurrently measured GPP (Fig.7). Analysis of residuals plots suggested that three of the data points (highlighted in red in Fig.7) might be considered outliers in the analysis, however, while removal of these outliers (not shown) improved R^2 from 0.37 to 0.68 it did not change the slope or intercept (at two decimal places).

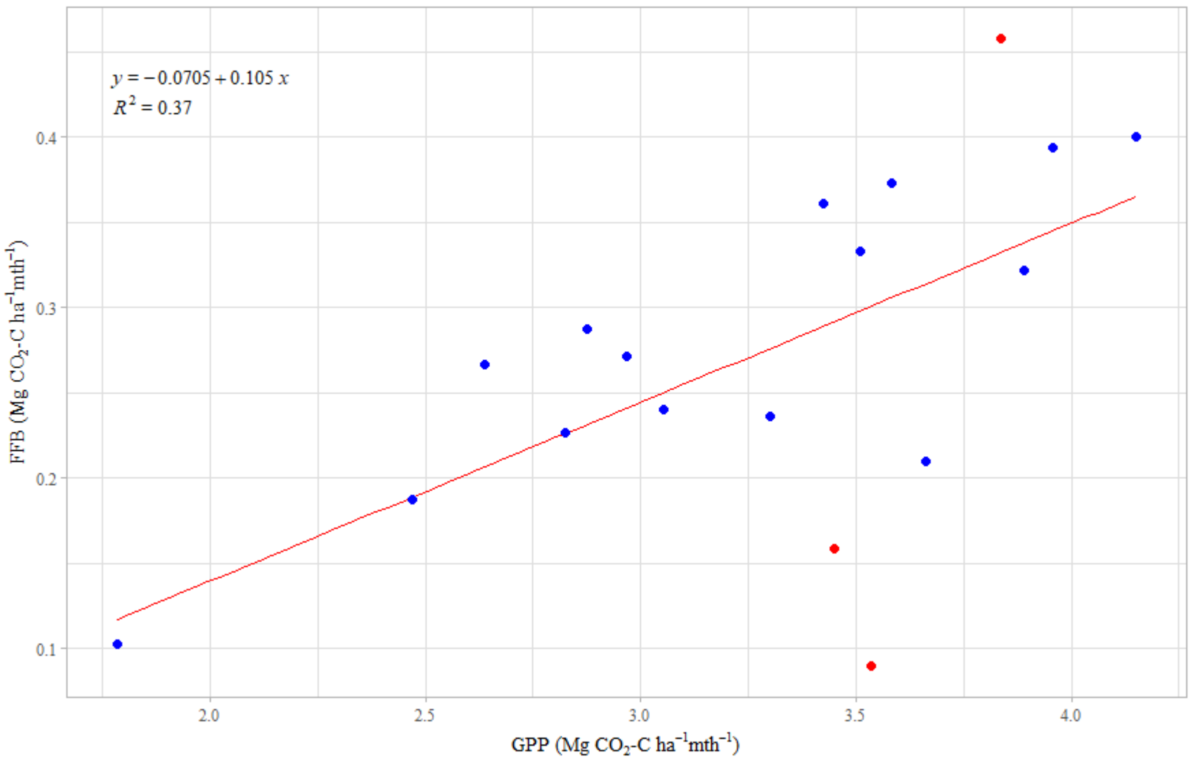

Figure 7: *Relationship between monthly GPP and FFB (Mg CO_2-C ha^{-1} mth^{-1}) for the years 2019/20 (GPP data for Mar to Jul 2019 are missing due to sensor failure). Red line shows the linear regression between the two parameters with the equation of the line and R^2 inset in the plot. Red points show data outliers (discussed in text)*

4 Discussion

In this study we have modelled photosynthetic uptake (GPP) across our range of measured water table depth and considered whether there was likely to be a significant yield penalty if WTD is moved closer to the soil surface than the industry standard of 0.6 m to reduce CO_2 emissions. We investigated this primarily by establishing the relationship between GPP and incoming light levels within water table depth bins across our recorded range and then using these derived parameters to estimate GPP if WTD was fixed to these bins across the entire dataset. GPP was initially partitioned from measured NEE (output from the Eddy Covariance technique) using a simple temperature response model for nighttime NEE (assumed to represent ecosystem respiration (Reco) as GPP = 0 at night), with daytime GPP then being calculated as the residual between NEE and extrapolated Reco. There are a range of approaches to EC flux partitioning, studies have utilised the nighttime NEE response to changing WTD itself as a model driver for ecosystem respiration in tropical peatland systems (e.g. Hirano et al., 2012, Deshmukh et al., 2021, McCalmont et al., 2021), though consideration is essential of both hysteresis and potential lags in this relationship since WTD indirectly covaries soil moisture content itself. Due to these lags and hysteresis effects, there may be substantial differences in soil CO_2 emission response to a particular WTD where this is found in a wetting or drying soil, and this may be further influenced by the time that the soil had spent in that particular state. As an alternative to nighttime NEE partitioning (whether correlating soil respiration with WTD or air temperature), the response of daytime NEE to incoming light levels (modulated by vapour pressure deficit) to estimate GPP is another standard approach (Lasslop et al., 2010). We employed this light response approach to partition daytime GPP in our previous study at this same site (McCalmont et al., 2021), making the assumption that the response of GPP to light levels would be a more reliable approach for accurate estimations of individual components of NEE at a tropical site with a limited temperature range. However, for the present study we considered that utilising parameters in partitioning that would later by used as regression model inputs (WTD, PPFD, diffFrac, VPD) would result in possible overfitting of the subsequent model. Therefore, in this present study, we make a simple partition of Reco (and therby GPP) using an Arrhenius type temperature response model on nighttime data (Lloyd & Taylor, 1994; Reichstein *et al.*, 2005). In conjunction with the temporal windows which are used for the nighttime partitioning (see Reichstein *et al.* (2005) for full details of this 'moving window' approach), the significant differences between the distribution of air temperatures within each WTD bin were sufficient to drive a strong enough response in night time respiration to allow reliable enough partitioning (effectively a data filter), whilst the temporal windows used in the partitioning are able accommodate hysteresis effects. We considered this a more cautious approach for this study where we are performing a comparison of dynamics within WTD bins, rather than establishing absolute values. The distribution of air temperatures within WTD bins, and statistical comparisons between them can be seen in Supplementary Materials Fig.S6. We did, however, also fit the same light response analyses to daytime partitioned GPP, and a comparison of the results of fitting to both of these derived datasets can be seen in Supplementary Materials Fig.S7. Results there show that the observed trends and conclusions remain robust between both day and nighttime partitioning methods.

Our initial, simple, regression modelling between GPP and FFB showed a very clear, direct, relationship between monthly photosynthetic uptake rate and fruit yield (Fig.7). The immediacy of this relationship may be considered remarkable in what might be expected to be a substantially lagged relationship (i.e., FFB production is likely to be the result of GPP accumulated over several weeks previously). Given our limited dataset of concurrent monthly FFB and GPP (and uncertainties in the specific timing of harvests in our commercial monthly yield data) it is difficult to draw too emphatic a conclusion from this simple regression, a much larger dataset (both spatially and temporally), or an isotopically labelled CO_2 field experiment, would be needed to confidently determine when carbon taken off in harvest was specifically assimilated, and quantify the relationship. However, the strong direct correlation between FFB and concurrently measured GPP was clear in our dataset and remained robust when compared to a range of lagged GPP scenarios (see Supplementary Materials Figs.S3 to S5). This correlation at the very least demonstrates the importance of GPP, the focus of our modelling, in FFB production.

Measured GPP within WTD data bins showed no significant differences within the upper 0-0.4 m of WTD, but deeper WTD (down to our measured limit of 0.6 m) resulted in lower CO_2 uptake into the palms (Fig.1). However, this was only shown to be significant when comparing WTD bins below 0.1 m, GPP rates from the shallowest (0 to 0.1 m) and the deepest (0.5 to 0.6 m) recorded WTD bins were not significantly different to each other. This result might suggest an optimum drainage depth somewhere between the two with GPP penalties from draining too shallow as well as too deep. This observation concurs with Henson *et al.* (2008) who reported that shallower water tables (provided roots were not permanently waterlogged) could aid yields by reducing leaching losses and minimizing the potential for soil water deficits. Certainly, our plantation block scale comparison of monthly yields and WTD drainage level would appear to circumstantially support the suggestion that WTD shallower than the industry standard of 0.6 m might be more optimal for production. Our study block was the most shallowly drained of all 43 blocks in the plantation (at an average of around 0.3 m), yet consistently recorded above average monthly yields (Fig. 2a and 2b).

However, to model GPP specifically and compare across our range of WTD bins, consideration was needed of the confounding effects of light quality and intensity and vapour pressure deficit which may be specific to individual WTD bin conditions. Using factor analysis to demonstrate the relative importance of the available variables, we showed the key role that light (both magnitude and quality), soil water status and atmospheric conditions (air temperature/vapour pressure deficit) play in photosynthetic uptake. Subsequently our light response modelling, showed that while WTD was an important parameter in GPP, there were substantial interactions with VPD and diffuse fraction of incoming light, indicating that they needed to be incorporated into our final, modified light response model.

Figure 4 shows that modelled GPP (fixed to the mean daytime value for PPFD at 824 μmol m^{-2} s^{-1}) was greater under more diffuse light conditions and reduced under greater VPD when considered across all WTD bins. These results estimated that overall GPP light use efficiency (μmol CO_2 μmol $PPFD^{-1}$) would be 27.5% greater under the 4th quartile of diffuse fraction compared to the 1st quartile. This figure is of a similar magnitude to the estimate of a diffuse light enhancement of 33% for a tropical broadleaf forest in Alton et al. (2007) who suggest that LAI (similar between oil palm and tropical broadleaf forest) would be a significant factor in determining canopy penetration of diffuse light.

We did not, however, see a clear trend of reducing GPP under increasing drainage depth (within our individual diffFrac and VPD quartiles (Fig.4), rather there appeared to be an optimum WTD level around 0.3 to 0.4 m (apparent in both nighttime and daytime partitioned datasets, fig. S7). This conclusion remained apparent after modifying our light response model to accommodate both diffFrac and VPD (Fig. 5c), GPP would be at its greatest with WTD between 0.3 to 0.4 m, a 3.6% increase compared to WTD at 0.5 to 0.6 m. From Fig.5a and Fig.5b we can see that this optimum drainage level for photosynthesis was due to a combination of improvements in both LUE and Amax; Amax was actually greater in the 0.2 to 0.3 m WTD bin, but LUE was lower here than at 0.3 to 0.4 m. It was the combination of the second greatest Amax and the greatest LUE that resulted in the 0.3 to 0.4 m WTD bin showing the greatest GPP. This was again reflected in our coefficient (k) which modifies the sensitivity of GPP to VPD, in this instance lower values of k result in higher modelled estimates for GPP; as can been seen in Table 2, the lowest value for k was seen with WTD at 0.3 to 0.4 m. We note, though, that error bars were particularly wide at the extremes of our somewhat limited WTD data range, (due to low numbers of data points) and that significant differences in GPP between WTD bins are therefore not emphatic. However, the lack of a clear GPP penalty with decreasing WTD would certainly suggest that raising WTD closer to the soil surface may be possible without substantial reductions in GPP. This result is broadly in agreement with manipulation experiments which saw optimum yields under WTD between 0.3 and 0.5 m (Othman *et al.*, 2011; Ginting & Darlan, 2016; Winarna *et al.*, 2017). However, while it has been reported that raising WTD from 0.6-0.7 m to 0.4-0.6 m could result in soil CO_2 emissions decreasing by 18% (Ginting & Darlan, 2016), our earlier results (McCalmont *et al.*, 2021) suggest emission reductions lower than this, though still substantial, reducing by 11% when

WTD is raised from 0.6 m to 0.4 m below the surface; our study showed that WTD would need to be reduced to 0.3 m to see a reduction in CO_2 emission of around 20%.

Our canopy modelling showed that the impact on GPP of increasing WTD was being reflected in reductions in canopy conductance and increased water management by the palms; the stomatal slope parameter (G1) is inversely correlated to the intrinsic water use efficiency (WUE) (Medlyn *et al.*, 2017). The observed reduction in G1 with increasing WTD (Fig.6) indicates greater stomatal sensitivity to VPD with deeper water tables. This was corroborated by similar reductions in atmospheric decoupling, as WTD increased Ω decreased, again indicating greater stomatal control of water flow through the palms. These reductions in stomatal conductance under increasing WTD, across our admittedly limited drainage range, do not, though, necessarily translate directly into reductions in GPP. More sophisticated canopy modelling (Meijide et al., 2017) has shown this decoupling between GPP and transpiration in oil palms with water use being relatively insensitive to variability in VPD or Rg (Röll et al., 2015), possibly linked to stem storage (and availability) of water. As reported in Dufrene and Saugier (1993), CO_2 uptake (GPP) remains resilient to reductions in stomatal conductance over a wide range of VPD conditions, with Amax not being significantly impacted until a VPD of around 1.8 kPa is reached. These levels of VPD were only exceeded for about 10% of our study period, (5% for >2kPa) so palm GPP remains notably resilient to current VPD conditions in this climatic region. However, the impact of WTD (and corresponding plant available water) on palm response and resilience to vapour pressure deficit is likely to become an ever more critical consideration as the climate warms in the coming decades, particularly in the free draining soils of peatland plantations. Global VPD, a function of air temperature, has increased exponentially since 1990, with projections of a continuation of this rise over the next 50 years (Yuan *et al.*, 2019) and is likely to become the dominant limiting factor in stomatal conductivity and evapotranspiration in many biomes (Novick *et al.*, 2016). Our canopy modelling suggests that bringing WTD closer to the soil surface would decrease water stress on the palms under these conditions, minimising the risk of longer-term hydraulic damage under drier atmospheric conditions (Grossiord *et al.*, 2017, Waite *et al.*, 2019).

5 Conclusion

For our site at least, significant yield penalties appear to be unlikely if mean WTD is reduced to limit peat CO_2 emission and our GPP modelling would suggest an optimum WTD depth at around 0.3 m. However, given our results are from a single site and our specific study block was not typical of the wider plantation, further studies are needed to validate these results more broadly. In particular, to determine whether these results persist at other sites and if they only occur when palms are established as seedlings at shallower levels of drainage or similar results would be seen when WTD is raised in mature stands. Future studies may begin to resolve this, where EC and WTD data are available from other peatland plantations similar analyses may be carried out to investigate whether those palms are also being stressed during conditions of deeper WTD, while insights from field studies might be gained from establishing long-term manipulation experiments where WTD is controlled at the block level and detailed yield series monitored.

6 Acknowledgements

The authors would like to thank the Director-General of the Malaysian Palm Oil Board (MPOB) for permission to publish these results. This study was carried out as part of a wider tropical peat research collaboration between MPOB, University of Exeter, University of Aberdeen and Newcastle University and we would like to thank the Sarawak Oil Palm Berhard (SOPB) for their help and support during the project. Specifically, at SOPB we would like to thank: Paul Wong Hee Kwong (group CEO), Chua Kian Hong (group plantation manager), Phang Seng Nam (regional plantation controller) and the Sabaju and Sebungan plantation managers for being kind enough to allow the research platform to be established within their plantations and the provision of logistical support when needed. At MPOB we would particularly like to thank the dedicated field technicians, without whose efforts and commitment this research would not have been possible, specifically Ham Jonathon, Muhammad Amira Ruzaizul Bin Bujang and Steward Saging. Finally, we would like to thank the anonymous reviewers for giving their valuable time to provide help and advice for the improvement of the paper.

7 Funding

The research was carried out as part of a project funded by the Malaysian Palm Oil Board (MPOB). The research was carried out with the support of Sarawak Oil Palm Berhard (SOPB) on whose land the research project was based.

8 References

ADHI, Y., MUBARAK, H., ROLAND, R., UTAMA, P., TAMBUSAI, N., ISMAIL, I., ANWAR, S., TARIGAN, S. & SAHARI, B. (2021) Effects of rainfall and groundwater level on soil subsidence, water content, and yield of oil palm. IOP Conference Series: Earth and Environmental Science, 2021. IOP Publishing, 012029.

ALTON, P., NORTH, P. & LOS, S. (2007). The impact of diffuse sunlight on canopy light-use efficiency, gross photosynthetic product and net ecosystem exchange in three forest biomes. *Global Change Biology,* 13**,** 776-787.

BALL, J. T., WOODROW, I. E. & BERRY, J. A. (1987). A model predicting stomatal conductance and its contribution to the control of photosynthesis under different environmental conditions. *In:* J., B. (ed.) *Progress in photosynthesis research.* Dordrecht: Springer.

BUSCH, J., FERRETTI-GALLON, K., ENGELMANN, J., WRIGHT, M., AUSTIN, K. G., STOLLE, F., TURUBANOVA, S., POTAPOV, P. V., MARGONO, B. & HANSEN, M. C. (2015). Reductions in emissions from deforestation from Indonesia's moratorium on new oil palm, timber, and logging concessions. *Proceedings of the National Academy of Sciences,* 112**,** 1328-1333.

CHEN, B., KENNEDY, C. M. & XU, B. (2019). Effective moratoria on land acquisitions reduce tropical deforestation: evidence from Indonesia. *Environmental Research Letters,* 14**,** 044009.

CHENG, S. J., BOHRER, G., STEINER, A. L., HOLLINGER, D. Y., SUYKER, A., PHILLIPS, R. P. & NADELHOFFER, K. J. (2015). Variations in the influence of diffuse light on gross primary productivity in temperate ecosystems. *Agricultural and Forest Meteorology,* 201**,** 98-110.

CHENG, Y., YU, L., XU, Y., LIU, X., LU, H., CRACKNELL, A. P., KANNIAH, K. & GONG, P. (2018). Towards global oil palm plantation mapping using remote-sensing data. *International Journal of Remote Sensing,* 39**,** 5891-5906.

COOK, S., WHELAN, M. J., EVANS, C. D., GAUCI, V., PEACOCK, M., GARNETT, M. H., KHO, L. K., TEH, Y. A. & PAGE, S. E. (2018). Fluvial organic carbon fluxes from oil palm plantations on tropical peatland. *Biogeosciences,* 15**,** 7435-7450.

COUWENBERG, J. & HOOIJER, A. (2013). Towards robust subsidence-based soil carbon emission factors for peat soils in south-east Asia, with special reference to oil palm plantations. *Mires & Peat,* 12.

DESHMUKH, C. S., JULIUS, D., DESAI, A. R., ASYHARI, A., PAGE, S. E., NARDI, N., SUSANTO, A. P., NURHOLIS, N., HENDRIZAL, M. & KURNIANTO, S. 2021. Conservation slows down emission increase from a tropical peatland in Indonesia. *Nature Geoscience***,** 1-7

DID (2001). Water Management Guidelines for Agricultural Development in Lowland Peat Swamps of Sarawak. Department of Irrigation and Drainage, Available on request at: https://did.sarawak.gov.my/page-0-0-381-Water-Management-Guidelines-for-Agricultural-Development-in-Lowland-Peat-Swamps-of-Sarawak.html#2

DUFRÊNE, E., DUBOS, B., REY, H., QUENCEZ, P. & SAUGIER, B. (1993). Changes in evapotranspiration from an oil palm stand (Elaeis guineensis Jacq.) exposed to seasonal soil water deficits. *Oléagineux (Paris),* 48**,** 105-120.

DUFRENE, E. & SAUGIER, B. (1993). Gas exchange of oil palm in relation to light, vapour pressure deficit, temperature and leaf age. *Functional Ecology*, 97-104.

GAVEAU, D. L., LOCATELLI, B., SALIM, M. A., YAEN, H., PACHECO, P. & SHEIL, D. (2018). Rise and fall of forest loss and industrial plantations in Borneo (2000–2017). *Conservation Letters*, e12622.

GINTING, E. & DARLAN, N. (2016) Effective water management for oil palm in Peatland: For peat conservation and yield optimization. 15TH International Peat Congress 2016.

GRÖMPING U., (2006). Relative Importance for Linear Regression in R: The Package relaimpo. Journal of Statistical Software, 17(1), 1--27

GROSSIORD, C., SEVANTO, S., BORREGO, I., CHAN, A. M., COLLINS, A. D., DICKMAN, L. T., HUDSON, P. J., MCBRANCH, N., MICHALETZ, S. T. & POCKMAN, W. T. (2017). Tree water dynamics in a drying and warming world. *Plant, cell & environment,* 40**,** 1861-1873.

GU, L., BALDOCCHI, D., VERMA, S. B., BLACK, T., VESALA, T., FALGE, E. M. & DOWTY, P. R. (2002). Advantages of diffuse radiation for terrestrial ecosystem productivity. *Journal of Geophysical Research: Atmospheres,* 107**,** ACL 2-1-ACL 2-23.

GUMBRICHT, T., ROMAN-CUESTA, R. M., VERCHOT, L., HEROLD, M., WITTMANN, F., HOUSEHOLDER, E., HEROLD, N. & MURDIYARSO, D. 2017. An expert system model for mapping tropical wetlands and peatlands reveals South America as the largest contributor. Global change biology, 23, 3581-3599.

HENSON, I. & MOHD, T. D. (2004). Seasonal variation in yield and developmental processes in an oil palm density trial on a peat soil: 1. Yield and bunch number components. *Journal of Oil Palm Research,* 16**,** 88-105.

HENSON, I. E. & CHANG, K. C. (2000). Oil palm productivity and its component processes. *Advances in oil palm research, Vol. 1***,** 97-145.

HENSON, I. E. & DOLMAT, M. T. (2003). Physiological analysis of an oil palm density trial on a peat soil. *Journal of Oil Palm Research,* 15.

HENSON, I. E., HARUN, M. H. & CHANG, K. (2008). Some observations on the effects of high water tables and flooding on oil palm, and a preliminary model of oil palm water balance and use in the presence of a high water table. *Oil Palm Bulletin,* 56**,** 14-22.

HIRANO, T., SEGAH, H., KUSIN, K., LIMIN, S., TAKAHASHI, H. & OSAKI, M. 2012. Effects of disturbances on the carbon balance of tropical peat swamp forests. *Global Change Biology,* 18**,** 3410-3422

HOLLINGER DY, KELLIHER FM, BYERS JN, HUNT JE, MCSEVERY TM, WEIR PL (1994) Carbon dioxide exchange between an undisturbed old-growth temperate forest and the atmosphere. Ecology, 75, 134–150

HOOIJER, A., PAGE, S., CANADELL, J. G., SILVIUS, M., KWADIJK, J., WÖSTEN, H. & JAUHIAINEN, J. (2010). Current and future CO_2 emissions from drained peatlands in Southeast Asia. *Biogeosciences,* 7**,** 1505-1514.

HUSNAIN, H., WIGENA, I. P., DARIAH, A., MARWANTO, S., SETYANTO, P. & AGUS, F. (2014). CO_2 emissions from tropical drained peat in Sumatra, Indonesia. *Mitigation and adaptation strategies for global change,* 19**,** 845-862.

ISHIKURA, K., HIRANO, T., OKIMOTO, Y., HIRATA, R., KIEW, F., MELLING, L., AERIES, E. B., SAN LO, K., MUSIN, K. K. & WAILI, J. W. (2018). Soil carbon dioxide emissions due to oxidative peat decomposition in an oil palm plantation on tropical peat. *Agriculture, Ecosystems & Environment,* 254**,** 202-212.

JARVIS, P. G. & MCNAUGHTON, K. G. (1986). Stomatal control of transpiration: scaling up from leaf to region. *Advances in ecological research,* 15**,** 1-49.

KALLARACKAL, J., JEYAKUMAR, P. & GEORGE, S. J. (2004). Water use of irrigated oil palm at three different arid locations in Peninsular India. *Journal of Oil Palm Research,* 16, 45-53.

KNAUER, J., EL-MADANY, T. S., ZAEHLE, S. & MIGLIAVACCA, M. (2018). Bigleaf—An R package for the calculation of physical and physiological ecosystem properties from eddy covariance data. *PLoS One,* 13, e0201114.

KNOHL, A. & BALDOCCHI, D. D. (2008). Effects of diffuse radiation on canopy gas exchange processes in a forest ecosystem. *Journal of Geophysical Research: Biogeosciences,* 113.

LASSLOP, G., REICHSTEIN, M., PAPALE, D., RICHARDSON, A. D., ARNETH, A., BARR, A., STOY, P. & WOHLFAHRT, G. (2010). Separation of net ecosystem exchange into assimilation and respiration using a light response curve approach: critical issues and global evaluation. *Global Change Biology,* 16, 187-208.

LEWIS, K., RUMPANG, E., KHO, L. K., MCCALMONT, J., TEH, Y. A., GALLEGO-SALA, A. & HILL, T. C. (2020). An assessment of oil palm plantation aboveground biomass stocks on tropical peat using destructive and non-destructive methods. *Scientific Reports,* 10, 1-12.

LLOYD, J. & TAYLOR, J. (1994). On the temperature dependence of soil respiration. *Functional ecology*, 315-323.

MANNING, F. C., KHO, L. K., HILL, T. C., CORNULIER, T. & TEH, Y. A. (2019). Carbon emissions from oil palm plantations on peat soil. *Frontiers in Forests and Global Change,* 2, 37.

MARWANTO, S. & AGUS, F. (2013). Is CO_2 flux from oil palm plantations on peatland controlled by soil moisture and/or soil and air temperatures? *Mitigation and Adaptation Strategies for Global Change,* 19, 809-819.

MARWANTO, S. & HENDRI, J. (2021). Excessive amount of rainfall decreases oil palm yield on well-drained peatland. IOP Conference Series: Earth and Environmental Science, 2021. IOP Publishing, 012099.

MCCALMONT, J., KHO, L. K., TEH, Y. A., LEWIS, K., CHOCHOLEK, M., RUMPANG, E. & HILL, T. (2021). Short-and long-term carbon emissions from oil palm plantations converted from logged tropical peat swamp forest. *Global Change Biology*. DOI: 10.1111/gcb.15544

MEDLYN, B. E., DE KAUWE, M. G., LIN, Y. S., KNAUER, J., DUURSMA, R. A., WILLIAMS, C. A., ARNETH, A., CLEMENT, R., ISAAC, P. & LIMOUSIN, J. M. (2017). How do leaf and ecosystem measures of water-use efficiency compare? *New Phytologist,* 216, 758-770.

ANA MEIJIDE, ALEXANDER RÖLL, YUANCHAO FAN, MATHIAS HERBST, FURONG NIU, FRANK TIEDEMANN, TANIA JUNE, ABDUL RAUF, DIRK HÖLSCHER, AND ALEXANDER KNOHL. 2017. "Controls of water and energy fluxes in oil palm plantations: Environmental variables and oil palm age." *Agricultural and Forest Meteorology*, 239, Pp. 71-85.

MIETTINEN, J., HOOIJER, A., VERNIMMEN, R., LIEW, S. C. & PAGE, S. E. (2017). From carbon sink to carbon source: extensive peat oxidation in insular Southeast Asia since 1990. *Environmental Research Letters,* 12.

MIETTINEN, J., SHI, C. & LIEW, S. C. (2016). Land cover distribution in the peatlands of Peninsular Malaysia, Sumatra and Borneo in 2015 with changes since 1990. *Global Ecology and Conservation,* 6, 67-78.

MONTAGNANI, L., GRÜNWALD, T., KOWALSKI, A., MAMMARELLA, I., MERBOLD, L., METZGER, S., SEDLÁK, P. & SIEBICKE, L. 2018. Estimating the storage term in eddy covariance measurements: the ICOS methodology. International Agrophysics, 32, 551-567.

NOVICK, K. A., FICKLIN, D. L., STOY, P. C., WILLIAMS, C. A., BOHRER, G., OISHI, A. C., PAPUGA, S. A., BLANKEN, P. D., NOORMETS, A. & SULMAN, B. N. (2016). The increasing importance of atmospheric demand for ecosystem water and carbon fluxes. *Nature climate change,* 6**,** 1023-1027.

OLIVEIRA, R. S., COSTA, F. R., VAN BAALEN, E., DE JONGE, A., BITTENCOURT, P. R., ALMANZA, Y., BARROS, F. D. V., CORDOBA, E. C., FAGUNDES, M. V. & GARCIA, S. (2019). Embolism resistance drives the distribution of Amazonian rainforest tree species along hydro-topographic gradients. *New Phytologist,* 221**,** 1457-1465.

OTHMAN, H., MOHAMMED, A. T., DARUS, F. M., HARUN, M. H. & ZAMBRI, M. P. (2011). Best management practices for oil palm cultivation on peat: ground water-table maintenance in relation to peat subsidence and estimation of CO_2 emissions at Sessang, Sarawak. *Journal of Oil Palm Research,* 23**,** 1078-1086.

PADFIELD, R., DREW, S., SYAYUTI, K., PAGE, S., EVERS, S., CAMPOS-ARCEIZ, A., KANGAYATKARASU, N., SAYOK, A., HANSEN, S. & SCHOUTEN, G. (2016). Landscapes in transition: an analysis of sustainable policy initiatives and emerging corporate commitments in the palm oil industry. *Landscape Research,* 41**,** 744-756.

PAGE, S. E., RIELEY, J. O. & BANKS, C. J. (2011). Global and regional importance of the tropical peatland carbon pool. *Global Change Biology,* 17**,** 798-818.

PERALTA-LOBO, F., VÁSQUEZ, O., RICHARDSON, D., ALVARADO-HERNÁNDEZ, A. & BORNEMISZA-STEINER, E. (1985). Effect of some soil physical characteristics on yield, growth and nutrition of the oil palm in Costa Rica. Effet de quelques caracteristiques physiques du sol sur le rendement, la croissance et la nutrition du palmier a huile au Costa Rica. *Oléagineux (Paris).* 40**,** 423-430.

PRANANTO, J. A., MINASNY, B., COMEAU, L. P., RUDIYANTO, R. & GRACE, P. (2020). Drainage increases CO_2 and N_2O emissions from tropical peat soils. *Global Change Biology,* 26**,** 4583-4600.

R CORE TEAM (2021). R: A language and environment for statistical computing. R Foundation for Statistical Computing, Vienna, Austria. URL https://www.R-project.org/

REICHSTEIN, M., FALGE, E., BALDOCCHI, D., PAPALE, D., AUBINET, M., BERBIGIER, P., BERNHOFER, C., BUCHMANN, N., GILMANOV, T. & GRANIER, A. (2005). On the separation of net ecosystem exchange into assimilation and ecosystem respiration: review and improved algorithm. *Global change biology,* 11**,** 1424-1439.

RÖLL, A., NIU, F., MEIJIDE, A., HARDANTO, A., HENDRAYANTO, KNOHL, A., HÖLSCHER, D., 2015.Transpiration in an oil palm landscape: effects of palm age. *Biogeosciences* 12,5619–5633, http://dx.doi.org/10.5194/bg-12-5619-2015.

ROWLAND, L., DA COSTA, A. C. L., GALBRAITH, D. R., OLIVEIRA, R., BINKS, O. J., OLIVEIRA, A., PULLEN, A., DOUGHTY, C. E., METCALFE, D. & VASCONCELOS, S. S. (2015). Death from drought in tropical forests is triggered by hydraulics not carbon starvation. *Nature,* 528**,** 119-122.

RSPO (2013). Round Table for Sustainable Palm Oil, Manual on Best Management Practices (BMPs). Available at: https://ledsgp.org/wp-content/uploads/2016/01/Summary-of-RSPO-Manual-on-BMP-for-Existing-Oil-Palm-Cultivation-on-Peat.pdf . Accessed on 05/05/2021

RSPO (2018). Round Table for Sustainable Palm Oil, Manual on Best Management Practices (BMPs). Available at: https://rspo.org/news-and-events/announcements/public-consultation-rspo-manuals-on-bmps-for-peat-existing-op-cultivation-and-rehabilitation-public-consultation-period-30102018-30112018 Accessed on: 28/10/2021

SANTIAGO, L. S., DE GUZMAN, M. E., BARALOTO, C., VOGENBERG, J. E., BRODIE, M., HÉRAULT, B., FORTUNEL, C. & BONAL, D. (2018). Coordination and trade-offs among hydraulic safety, efficiency and drought avoidance traits in Amazonian rainforest canopy tree species. *New Phytologist,* 218**,** 1015-1024.

SCHARLEMANN, J. P., TANNER, E. V., HIEDERER, R. & KAPOS, V. (2014). Global soil carbon: understanding and managing the largest terrestrial carbon pool. *Carbon Management,* 5**,** 81-91.

SMITH, B. (1989). The effects of soil water and atmospheric vapour pressure deficit on stomatal behaviour and photosynthesis in the oil palm. *Journal of Experimental Botany,* 40**,** 647-651.

SPIESS, A.N., (2018). propagate: Propagation of Uncertainty. R package version 1.0-6. https://CRAN.R-project.org/package=propagate

WAITE, P.-A., SCHULDT, B., MATHIAS LINK, R., BREIDENBACH, N., TRIADIATI, T., HENNINGS, N., SAAD, A. & LEUSCHNER, C. (2019). Soil moisture regime and palm height influence embolism resistance in oil palm. *Tree physiology,* 39**,** 1696-1712.

WANG, X., WU, J., CHEN, M., XU, X., WANG, Z., WANG, B., WANG, C., PIAO, S., LIN, W. & MIAO, G. (2018). Field evidences for the positive effects of aerosols on tree growth. *Global change biology,* 24**,** 4983-4992.

WINARNA, W., YUSUF, M. A., RAHUTOMO, S. & SUTARTA, E. S. (2017). Impacts of water table and soil ameliorant on soil moisture, CO_2 emission, and oil palm yield on peat soil. *Jurnal Penelitian Kelapa Sawit,* 25**,** 147-160.

WOITTIEZ L.S., MARK T. VAN WIJK M. T., SLINGERLAND M., VAN NOORDWIJK M., GILLER K.E. (2017) Yield gaps in oil palm: A quantitative review of contributing factors. *European Journal of Agronomy*. 83, 57-77. ISSN 1161-0301. https://doi.org/10.1016/j.eja.2016.11.002.

YUAN, W., ZHENG, Y., PIAO, S., CIAIS, P., LOMBARDOZZI, D., WANG, Y., RYU, Y., CHEN, G., DONG, W. & HU, Z. (2019). Increased atmospheric vapor pressure deficit reduces global vegetation growth. *Science advances,* 5**,** eaax1396.

ZHANG, Y., BASTOS, A., MAIGNAN, F., GOLL, D., BOUCHER, O., LI, L., CESCATTI, A., VUICHARD, N., CHEN, X. & AMMANN, C. (2020). Modeling the impacts of diffuse light fraction on photosynthesis in ORCHIDEE (v5453) land surface model. *Geoscientific Model Development,* 13**,** 5401-5423.

Oil palm (*Elaeis guineensis*) plantation on tropical peatland in South East Asia: photosynthetic response to soil drainage level for mitigation of soil carbon emissions

Supplementary Materials

GPP measured within WTD bins

Table S1. *Mean and median GPP flux rates per water table depth (WTD) bin*

Water table depth [m]	GPP (mean) [µmol m-2 s^{-1}]	GPP (median) [µmol m-2 s^{-1}]	n()
[0.0,0.1]	26.42 ± 0.3	27.75	1000
[0.1,0.2]	26.68 ± 0.2	27.78	3812
[0.2,0.3]	27.41 ± 0.1	28.15	4860
[0.3,0.4]	27.50 ± 0.2	28.07	2350
[0.4,0.5]	25.41 ± 0.3	25.87	1543
[0.5,0.6]	25.63 ± 0.5	26.07	457

± standard error

Factor Analysis

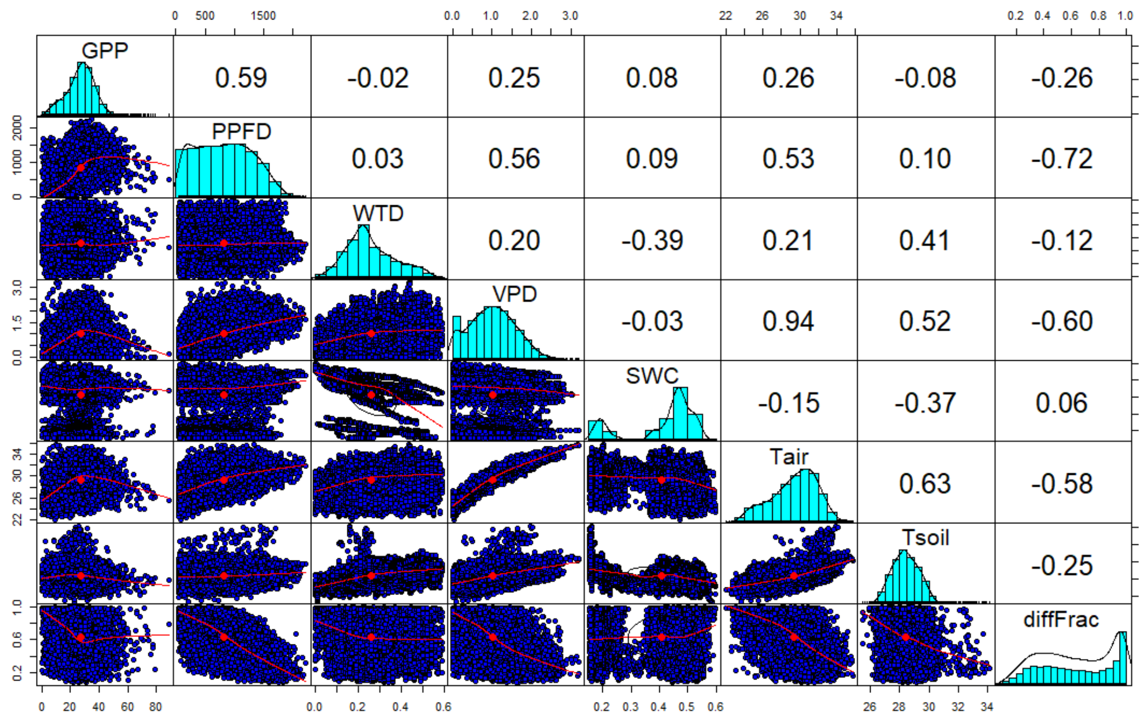

Figure S1. *Pearson's correlation matrix showing co-linearity between variable measured in the study.*

Table S2. *Correlation of each PC to GPP, in order of importance*

Factor	GPP	PC6	PC2	PC1	PC3	PC5	PC7	PC4
Correlation coefficient	1.00	0.35	0.33	0.29	-0.23	0.19	0.14	-0.03

Regression model summary:

Residuals:

Min	**1Q**	**Median**	**3Q**	**Max**
-39.332	-4.454	-0.028	4.240	66.784

Coefficients:

	Estimate	**Std. Error**	**t value**	**Pr(>|t|)**
(Intercept)	26.87932	0.06456	416.335	< 2e-16 ***
PC1	1.62303	0.03524	46.060	< 2e-16 ***
PC2	2.64603	0.05065	52.243	< 2e-16 ***
PC3	-2.65649	0.07288	-36.450	< 2e-16 ***
PC4	-0.34902	0.08258	-4.226	2.39e-05 ***
PC5	3.47989	0.11276	30.861	< 2e-16 ***
PC6	7.12161	0.12847	55.432	< 2e-16 ***
PC7	7.10978	0.31748	22.395	< 2e-16 ***

Residual standard error: 7.645 on 14014 degrees of freedom

Multiple R-squared: 0.4335, Adjusted R-squared: 0.4332

F-statistic: 1532 on 7 and 14014 DF, p-value: < 2.2e-16

Relative importance of PCs in regression model

	%	**cumul** %		**Lower** 0.95	**Upper** 0.95
PC6.lmg	28.65	28.65	A______	26.81	30.55
PC2.lmg	25.45	54.10	_B_____	23.66	27.16
PC1.lmg	19.78	73.88	__C____	18.18	21.43
PC3.lmg	12.39	86.27	___D___	10.79	14.00
PC5.lmg	08.88	95.15	____E__	07.87	10.03
PC7.lmg	04.68	99.83	_____F_	03.80	05.61
PC4.lmg	00.17	100.0	______G	00.04	00.37

Light Response curves

Table S3. *Light use efficiency (**LUE**), maximum assimilation (**Amax**) with associated model fit statistics (t stat and p values) and predicted photosynthetic uptake (**GPP**) within water table depth (**WTD**) and light quality (**diffuse fraction**) bins. ± values show standard errors of the model fit, values in square brackets for predicted GPP show 95% confidence intervals. n() shows number of data points available in each data bin*

WTD [m]	Diffuse fraction	LUE [µmol CO_2 µmol^{-1} PPFD]	LUE (t_stat[p_val])	Amax [µmol CO_2 m$_{-2}$ s$_{-1}$]	Amax (t_stat[p_val])	Predicted GPP [µmol CO_2 m^{-2} s^{-1}]	n()
[0.0,0.1]	**[1st_quartile]**	0.14 ± 0.064	2.21 [<0.05]	33.41 ± 3.28	10.19 [<0.0001]	25.93 [9.94, 27.03]	116
[0.1,0.2]	**[1st_quartile]**	0.09 ± 0.011	8.26 [<0.0001]	38.67 ± 1.59	24.28 [<0.0001]	25.38 [23.84, 25.96]	830
[0.2,0.3]	**[1st_quartile]**	0.11 ± 0.009	12.05 [<0.0001]	38.44 ± 0.95	40.37 [<0.0001]	26.72 [25.92, 27.13]	1331
[0.3,0.4]	**[1st_quartile]**	0.11 ± 0.013	8.48 [<0.0001]	38.28 ± 1.28	29.94 [<0.0001]	26.95 [25.65, 27.49]	641
[0.4,0.5]	**[1st_quartile]**	0.08 ± 0.013	6.42 [<0.0001]	36.98 ± 2.25	16.45 [<0.0001]	23.84 [21.89, 24.53]	485
[0.5,0.6]	**[1st_quartile]**	0.24 ± 0.106	2.27 [<0.05]	30.16 ± 1.72	17.49 [<0.0001]	26.17 [16.18, 27.12]	103
[0.0,0.1]	**[2nd_quartile]**	0.08 ± 0.009	8.40 [<0.0001]	51.45 ± 3.69	13.94 [<0.0001]	28.79 [26.87, 29.58]	170
[0.1,0.2]	**[2nd_quartile]**	0.08 ± 0.005	16.98 [<0.0001]	50.02 ± 1.81	27.69 [<0.0001]	28.30 [27.62, 28.72]	939
[0.2,0.3]	**[2nd_quartile]**	0.09 ± 0.005	18.02 [<0.0001]	48.06 ± 1.36	35.42 [<0.0001]	29.72 [29.13, 30.14]	1192
[0.3,0.4]	**[2nd_quartile]**	0.12 ± 0.009	13.21 [<0.0001]	43.97 ± 1.32	33.39 [<0.0001]	30.21 [29.48, 30.69]	668
[0.4,0.5]	**[2nd_quartile]**	0.09 ± 0.010	9.24 [<0.0001]	46.48 ± 2.67	17.43 [<0.0001]	28.55 [27.17, 29.27]	409
[0.5,0.6]	**[2nd_quartile]**	0.1 ± 0.014	7.00 [<0.0001]	47.58 ± 3.34	14.25 [<0.0001]	29.92 [27.79, 30.93]	127
[0.0,0.1]	**[3rd_quartile]**	0.11 ± 0.008	13.10 [<0.0001]	52.65 ± 2.47	21.34 [<0.0001]	33.09 [32.14, 33.75]	310
[0.1,0.2]	**[3rd_quartile]**	0.1 ± 0.005	21.72 [<0.0001]	52.76 ± 1.61	32.68 [<0.0001]	32.58 [32.05, 33.02]	978
[0.2,0.3]	**[3rd_quartile]**	0.12 ± 0.006	21.15 [<0.0001]	48.89 ± 1.23	39.90 [<0.0001]	32.97 [32.44, 33.41]	1213
[0.3,0.4]	**[3rd_quartile]**	0.11 ± 0.007	15.77 [<0.0001]	51.64 ± 2.09	24.77 [<0.0001]	33.18 [32.32, 33.83]	535
[0.4,0.5]	**[3rd_quartile]**	0.12 ± 0.012	10.71 [<0.0001]	42.63 ± 2.07	20.64 [<0.0001]	30.13 [28.94, 30.97]	350
[0.5,0.6]	**[3rd_quartile]**	0.09 ± 0.012	7.30 [<0.0001]	52.89 ± 5.82	9.08 [<0.0001]	30.89 [28.19, 32.16]	119
[0.0,0.1]	**[4th_quartile]**	0.11 ± 0.006	17.76 [<0.0001]	52.56 ± 2.7	19.45 [<0.0001]	33.23 [31.9, 34.18]	404
[0.1,0.2]	**[4th_quartile]**	0.12 ± 0.004	27.74 [<0.0001]	50.79 ± 1.63	31.17 [<0.0001]	33.64 [32.76, 34.37]	1065
[0.2,0.3]	**[4th_quartile]**	0.12 ± 0.005	25.45 [<0.0001]	47.8 ± 1.57	30.39 [<0.0001]	32.45 [31.51, 33.19]	1124
[0.3,0.4]	**[4th_quartile]**	0.12 ± 0.006	19.27 [<0.0001]	53.12 ± 2.67	19.86 [<0.0001]	34.08 [32.64, 35.14]	506
[0.4,0.5]	**[4th_quartile]**	0.14 ± 0.012	11.8 [<0.0001]	42.56 ± 2.71	15.67 [<0.0001]	31.07 [28.98, 32.54]	299
[0.5,0.6]	**[4th_quartile]**	0.13 ± 0.014	9.73 [<0.0001]	47.42 ± 3.99	11.88 [<0.0001]	33.11 [30.23, 35.01]	108

Table S4. *Light use efficiency (**LUE**), maximum assimilation (**Amax**) with associated model fit statistics (t stat and p values) and predicted photosynthetic uptake (**GPP**) within water table depth (**WTD**) and vapour pressure deficit (**VPD**) bins. ± values show standard errors of the model fit, values in square brackets for predicted GPP show 95% confidence intervals. n() shows number of data points available in each data bin*

WTD [m]	Vapour pressure deficit	LUE [µmol CO_2 µmol^{-1} PPFD]	LUE (t_stat[p_val])	Amax [µmol CO_2 m_{-2} s_{-1}]	Amax (t_stat[p_val])	Predicted GPP [µmol CO_2 m^{-2} s^{-1}]	n()
[0,0.1]	**[1st_quartile]**	0.11 ± 0.01	15.63 [<0.0001]	48.52 ± 2.41	20.15 [<0.0001]	31.70 [30.46, 32.63]	411
[0.1,0.2]	**[1st_quartile]**	0.13 ± 0.01	21.20 [<0.0001]	45.37 ± 1.49	30.45 [<0.0001]	31.70 [30.82, 32.44]	1088
[0.2,0.3]	**[1st_quartile]**	0.12 ± 0.01	18.98 [<0.0001]	47.7 ± 1.84	25.94 [<0.0001]	32.59 [31.55, 33.42]	1129
[0.3,0.4]	**[1st_quartile]**	0.12 ± 0.01	13.32 [<0.0001]	50.71 ± 3.03	16.73 [<0.0001]	33.41 [31.74, 34.65]	463
[0.4,0.5]	**[1st_quartile]**	0.18 ± 0.02	7.20 [<0.0001]	36.82 ± 2.61	14.11 [<0.0001]	29.37 [26.83, 31.1]	308
[0.5,0.6]	**[1st_quartile]**	0.12 ± 0.02	5.85 [<0.0001]	47.08 ± 6.32	7.45 [<0.0001]	31.89 [27.02, 34.41]	107
[0,0.1]	**[2nd_quartile]**	0.13 ± 0.01	12.57 [<0.0001]	45.37 ± 1.55	29.33 [<0.0001]	32.21 [31.36, 32.84]	334
[0.1,0.2]	**[2nd_quartile]**	0.12 ± 0.01	21.46 [<0.0001]	45.27 ± 0.97	46.85 [<0.0001]	31.35 [30.88, 31.76]	1088
[0.2,0.3]	**[2nd_quartile]**	0.13 ± 0.01	20.38 [<0.0001]	44.84 ± 0.98	45.64 [<0.0001]	31.27 [30.77, 31.71]	1122
[0.3,0.4]	**[2nd_quartile]**	0.15 ± 0.01	15.80 [<0.0001]	42.51 ± 1.06	40.08 [<0.0001]	31.49 [30.84, 32.05]	539
[0.4,0.5]	**[2nd_quartile]**	0.12 ± 0.01	10.19 [<0.0001]	44.27 ± 2.18	20.28 [<0.0001]	30.29 [29.12, 31.12]	320
[0.5,0.6]	**[2nd_quartile]**	0.12 ± 0.02	7.08 [<0.0001]	46.26 ± 3.38	13.69 [<0.0001]	31.75 [29.65, 32.96]	102
[0,0.1]	**[3rd_quartile]**	0.15 ± 0.03	5.96 [<0.0001]	39.73 ± 1.93	20.62 [<0.0001]	30.06 [28.22, 30.94]	195
[0.1,0.2]	**[3rd_quartile]**	0.13 ± 0.01	14.23 [<0.0001]	39.8 ± 0.94	42.47 [<0.0001]	28.72 [28.13, 29.17]	962
[0.2,0.3]	**[3rd_quartile]**	0.12 ± 0.01	21.66 [<0.0001]	42.69 ± 0.74	57.98 [<0.0001]	29.96 [29.55, 30.3]	1301
[0.3,0.4]	**[3rd_quartile]**	0.12 ± 0.01	16.09 [<0.0001]	42.5 ± 1.04	40.87 [<0.0001]	30.00 [29.41, 30.47]	596
[0.4,0.5]	**[3rd_quartile]**	0.11 ± 0.01	9.56 [<0.0001]	41.8 ± 1.91	21.85 [<0.0001]	28.2 [27.02, 28.96]	342
[0.5,0.6]	**[3rd_quartile]**	0.11 ± 0.02	6.99 [<0.0001]	41.39 ± 2.46	16.82 [<0.0001]	28.6 [26.81, 29.59]	109
[0,0.1]	**[4th_quartile]**	0.36 ± 0.33	1.09 [<0.0001]	29.69 ± 2.39	12.41 [<0.0001]	26.97 [-1.76, 61.85]	60
[0.1,0.2]	**[4th_quartile]**	0.15 ± 0.02	8.12 [<0.0001]	35.00 ± 0.94	37.34 [<0.0001]	27.26 [26.28, 27.74]	674
[0.2,0.3]	**[4th_quartile]**	0.17 ± 0.01	11.68 [<0.0001]	35.78 ± 0.64	55.75 [<0.0001]	28.36 [27.79, 28.71]	1308
[0.3,0.4]	**[4th_quartile]**	0.16 ± 0.02	10.42 [<0.0001]	36.83 ± 0.81	45.74 [<0.0001]	28.66 [27.94, 29.09]	752
[0.4,0.5]	**[4th_quartile]**	0.11 ± 0.01	9.30 [<0.0001]	34.78 ± 1.14	30.60 [<0.0001]	25.28 [24.42, 25.77]	573
[0.5,0.6]	**[4th_quartile]**	0.18 ± 0.03	6.08 [<0.0001]	33.92 ± 1.21	28.08 [<0.0001]	27.56 [26.29, 28.3]	139

Table S5. Mean PPFD, VPD and diffuse fraction of incoming light found within each water table bin (WTD)

WTD bin [m]	PPFD [µmol m^{-2} s^{-1}]	VPD [kPa]	Diffuse Fraction
[0,0.1]	**709.63** ± 13.45	**0.70** ± 0.01	**0.76** ± 0.01
[0.1,0.2]	**811.25** ± 7.75	**0.91** ± 0.01	**0.66** ± 0.00
[0.2,0.3]	**850.66** ± 6.99	**1.05** ± 0.01	**0.62** ± 0.00
[0.3,0.4]	**849.17** ± 9.91	**1.14** ± 0.01	**0.61** ± 0.01
[0.4,0.5]	**831.32** ± 11.85	**1.21** ± 0.02	**0.58** ± 0.01
[0.5,0.6]	**766.84** ± 21.84	**1.10** ± 0.03	**0.64** ± 0.01

± S.E.

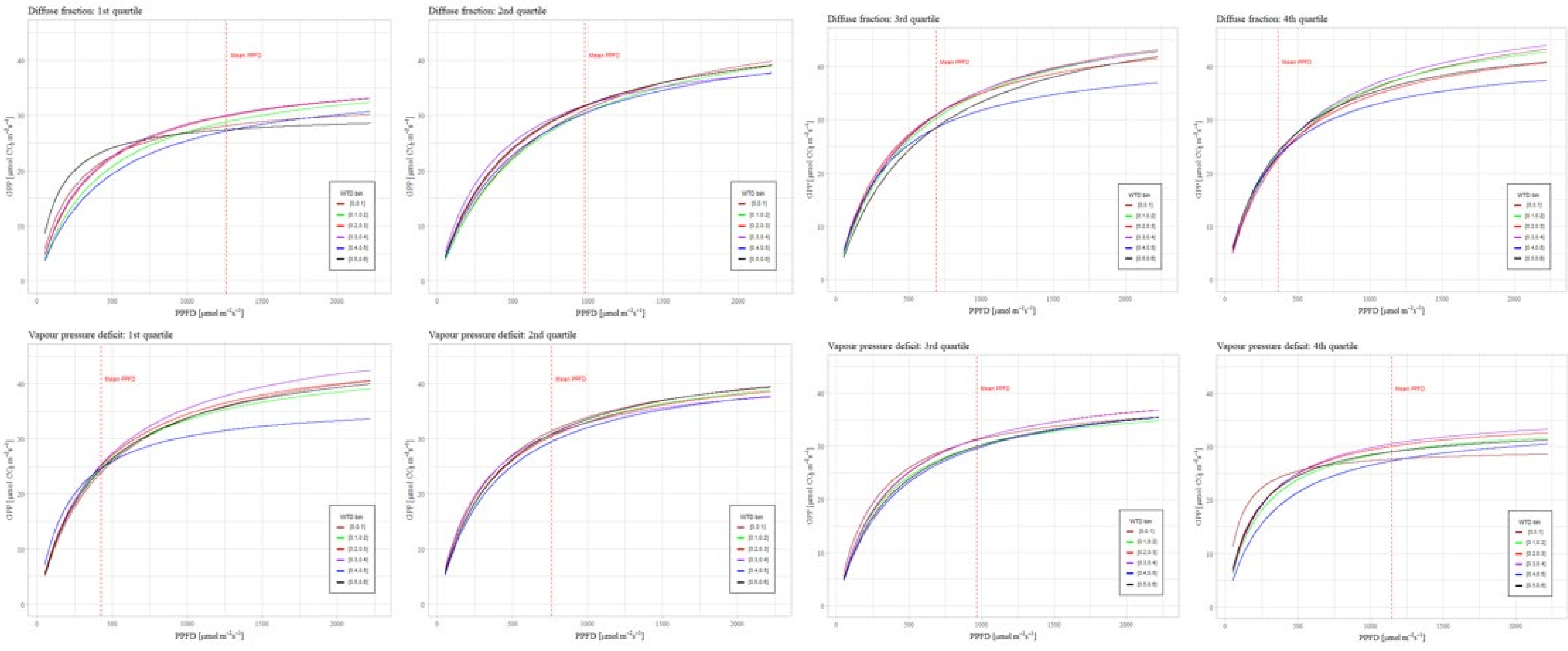

Figure S2. *Light response curves, comparison between WTD bins within quartiles of light quality (diffuse fraction), upper plots, and vapour pressure deficit (lower plots). Dashed red line in each plot shows the mean PPFD found within each specific data quartile.*

Canopy modelling

Table S6. *Atmospheric decoupling coefficient (**Ω**) and stomatal slope parameter (**G1**) compared between WTD bins. Ω shows the mean (± standard error) of values calculated for each half hour timestep within WTD bins. G1 (and associated t and p statistics) shows the slope of the non-linear regression between canopy conductance and normalised GPP, fitted within individual WTD bins (± the standard error of the parameter estimates). n() shows the number of data points available for model fitting within each WTD bin.*

WTD [m]	Ω	G1	G1 [t_stat]	G1 [Pr(>|t|)]	n()
[0,0.1]	0.63 ± 0.03	9.66 ± 2.6	3.71	5.82E-04	45
[0.1,0.2]	0.59 ± 0.01	8.33 ± 0.31	26.45	3.31E-114	891
[0.2,0.3]	0.58 ± 0.01	7.53 ± 0.19	40.5	7.37E-258	1866
[0.3,0.4]	0.57 ± 0.01	7.33 ± 0.28	25.88	2.58E-113	995
[0.4,0.5]	0.53 ± 0.01	7.05 ± 0.17	41.72	1.03E-209	870
[0.5,0.6]	0.52 ± 0.01	6.37 ± 0.28	23.12	1.33E-61	228

Supplementary Equations

Equations implemented using R package 'Bigleaf' (Knauer et al., 2018)

Equation S1: (Monteith, 2008)

$$G_{ah} = \frac{1}{{}^{1}/_{G_{am}} + {}^{1}/_{G_b}}$$

Where:

G_{ah} = *aerodynamic conductance for heat (m s^{-1})*

G_{am} = *aerodynamic conductance for momentum (m s^{-1})*

G_b = *canopy boundary layer conductance (m s^{-1})*

Equation S2: (Monteith, 2008)

$$G_{am} = \frac{u_*^2}{u(z_r)}$$

Where:

G_{am} = *aerodynamic conductance for momentum (m s^{-1})*

u_* = *friction velocity (m s^{-1})*

$u(z_r)$ = *horizontal wind speed at measurement height (m s^{-1})*

Equation S3: (Thom, 1972)

$$G_b = (6.2 \cdot u_*^{-0.67})^{-1}$$

Where:

G_b = *canopy boundary layer conductance (m s^{-1})*

u_* = *friction velocity (m s^{-1})*

Equation S4: (Monteith, 1965)

$$G_{sw} = \frac{LE \cdot G_{ah} \cdot \gamma}{s \cdot (Rn - G - S) + \rho \cdot c_p \cdot G_{ah} \cdot VPD - LE(s + \gamma)}$$

Where:

G_{sw} = *Canopy conductance for water vapour (m s^{-1})*

LE = *latent energy (W m^{-2})*

G_{ah} = *Aerodynamic conductance for heat (m s^{-1})*

γ = *psychrometric constant (kPa degC^{-1})*

s = *slope of saturation vapour pressure curve (kPa degC^{-1})*

Rn = *net radiation (W m^{-2})*

G = *ground heat flux (W m^{-2})*

S = *sum of all energy storage fluxes (W m^{-2})*

ρ = *air density (kg m^{-3})*

cp = *heat capacity of dry air (J degC^{-2} kg^{-1})*

VPD = *vapour pressure deficit (kPa)*

Bulk transfer equations for sensible and latent heat

Equation S5:

$$T_{surf} = T_{air} + H/(\rho \cdot cp \cdot Ga)$$

Where:

T_{surf} = *air temperature at canopy surface (degC)*

T_{air} = *air temperature at measurement height (degC)*

H = *sensible heat ($W\ m^{-2}$)*

ρ = *air density ($kg\ m^{-3}$)*

cp = *heat capacity of dry air ($J\ degC^{-2}\ kg^{-1}$)*

G_{ah} = *aerodynamic conductance for heat ($m\ s^{-1}$)*

Equation S6:

$$e_{surf} = e + (LE \cdot \gamma)/(Ga \cdot \rho \cdot cp)$$

Where:

e_{surf} = *vapour pressure at canopy surface (kPa)*

e = *vapour pressure at measurement height (kPa)*

LE = *latent energy ($W\ m^{-2}$)*

γ = *psychrometric constant ($kPa\ degC^{-1}$)*

G_{ah} = *aerodynamic conductance for heat ($m\ s^{-1}$)*

ρ = *air density ($kg\ m^{-3}$)*

cp = *heat capacity of dry air ($J\ degC^{-2}\ kg^{-1}$)*

Equation S7: (Sonntag 1990)

$$esat_{surf} = \frac{611.2\ \cdot \exp\left((17.62 \cdot T_{surf})/(243.12 + T_{surf}\right)}{1000}$$

Where:

***esat**$_{surf}$* = *saturation vapour pressure at canopy surface (kPa)*

***T**$_{surf}$* = *air temperature at canopy surface (degC)*

Equation S8:

$$VPD_{surf} = esat_{surf} - e_{surf}$$

Where:

***VPD**$_{surf}$*	=	*vapour pressure deficit at surface (kPa)*
***esat**$_{surf}$*	=	*saturation vapour pressure deficit at the surface (kPa)*
***e**$_{surf}$*	=	*vapour pressure at canopy surface (kPa)*

Equation S9:

$$Ca_{surf} = Ca + NEE/Ga_{CO_2}$$

Where:

***Ca**$_{surf}$*	=	*CO_2 concentration at the surface (μmol mol^{-1})*
Ca	=	*CO_2 concentration at measurement height (μmol mol^{-1})*
NEE	=	*net ecosystem exchange of CO_2 (μmol CO_2 m^{-2} s^{-1})*
***Ga**$_{CO2}$*	=	*aerodynamic conductance for CO_2 (m s^{-1})*

Equation S10:

$$Ga_{CO2} = \frac{1}{Ra_m + 1/Gb_{CO2}}$$

Where:

***Ra**$_m$ = **1/Ga**$_m$* *(Eq. S2) canopy boundary layer resistance to momentum (m s^{-1})*

***Gb**$_{CO2}$* = *canopy boundary layer conductance for CO2 (Eq. S11)*

Equation S11:

$$Gb_{CO2} = \frac{G_b}{(\frac{1.07}{0.71})^\wedge 0.67}$$

Where:

G_b = *canopy boundary layer conductance (m s^{-1}) (Eq. S3)*

Comparison of regressions of monthly fresh fruit bunch (FFB) production and photosynthetic uptake (GPP)

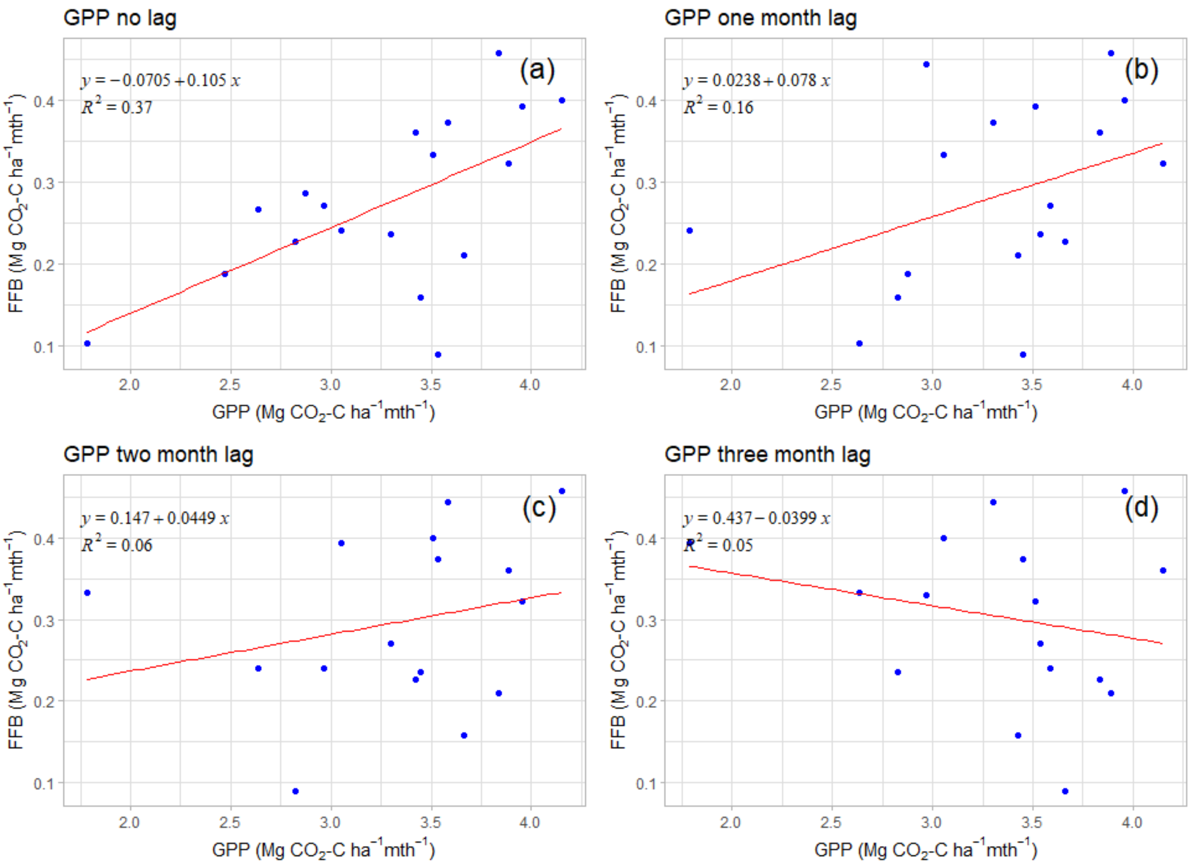

Figure S3 *Comparison of concurrently measured GPP~FFB (GPP no lag) with lagged GPP:* ***(a)****: FFB at month[x] vs GPP at month[x],* ***(b)****: GPP at month [x-1],* ***(c)****: GPP at month[x-2],* ***(d)****: GPP at month[x-3].*

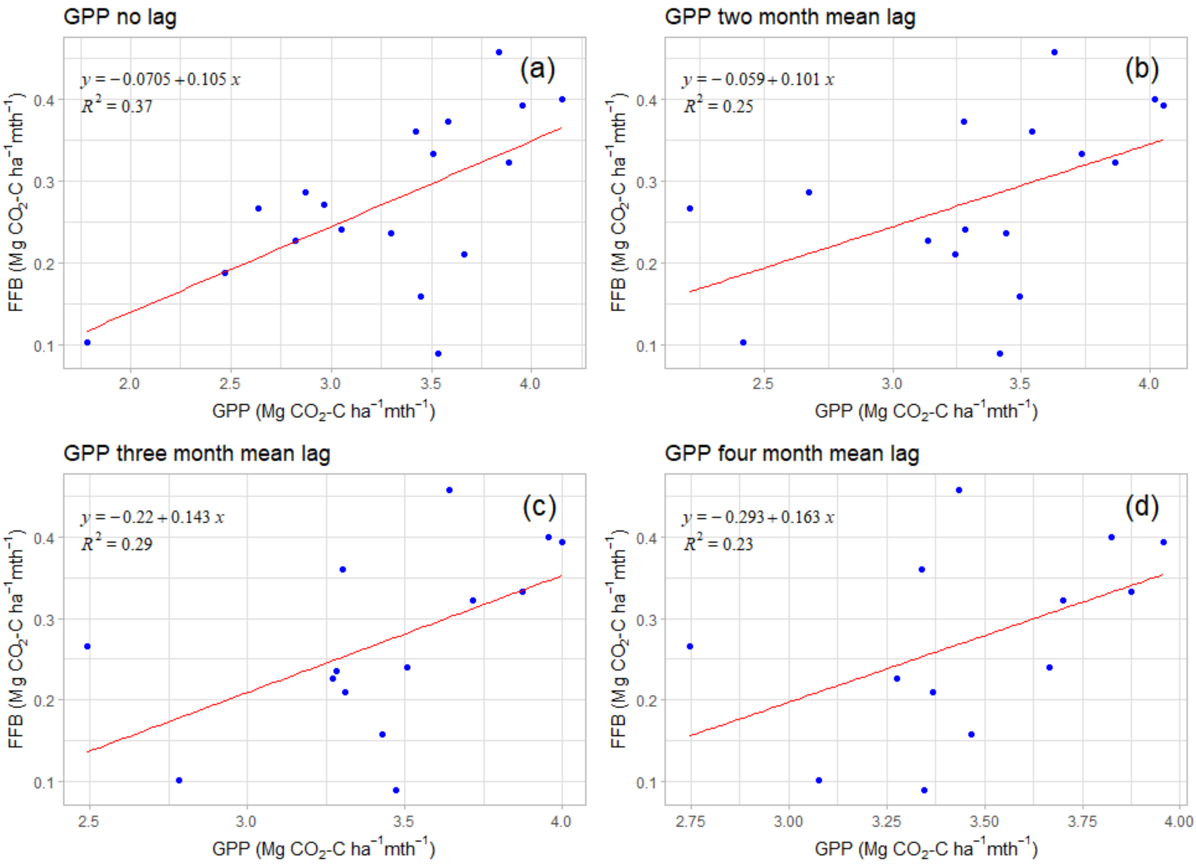

Figure S4. *Comparison of concurrently measured GPP~FFB (GPP no lag) with lagged scenarios of mean GPP:* ***(a)****: FFB at month[x] vs GPP at month[x],* ***(b)****: GPP mean of months[x, x-1],* ***(c)****: GPP mean of months[x, x-1, x-2],* ***(d)****: GPP mean of months[x, x-1, x-2, x-3].*

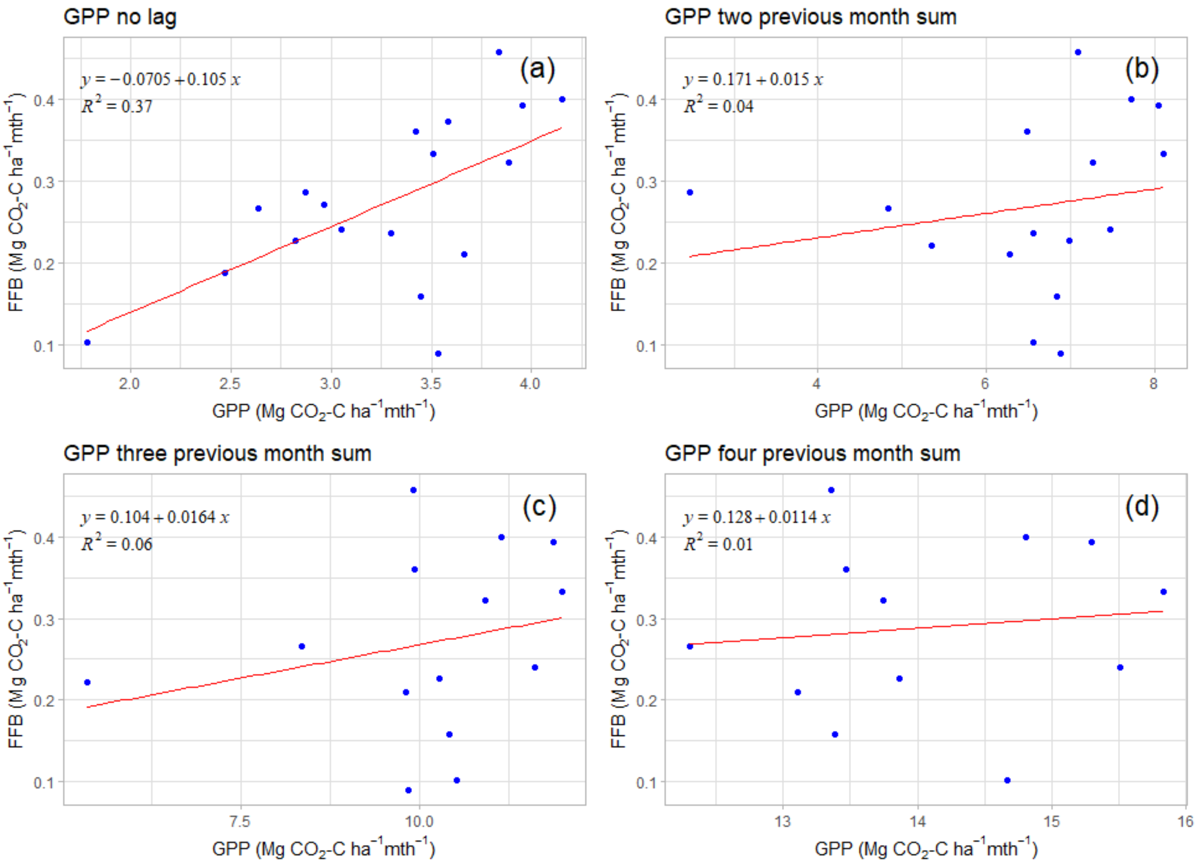

Figure S5. *Comparison of concurrently measured GPP~FFB (GPP no lag) with lagged scenarios of summed GPP:* ***(a)****: FFB at month[x] vs GPP at month[x],* ***(b)****: GPP sum of months[x, x-1],* ***(c)****: GPP sum of months[x, x-1, x-2],* ***(d)****: GPP sum of months[x, x-1, x-2, x-3].*

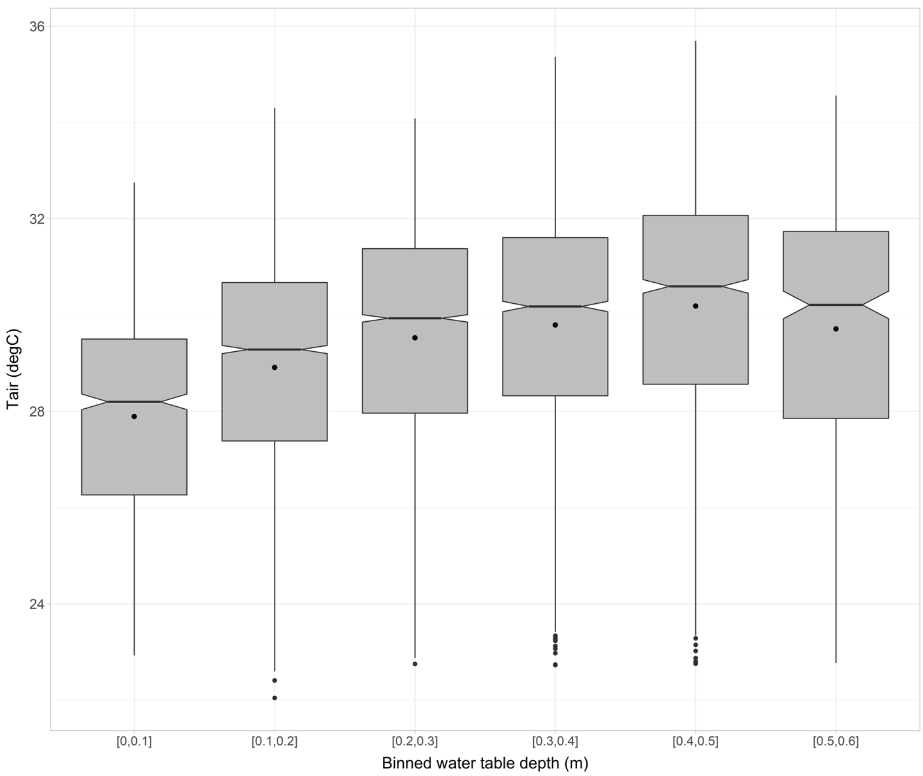

Figure S6. *Distribution of air temperature within WTD bins, horizontal lines show median values for each bin with notches indicating the 95% confidence intervals (1.5 * IQR/n, overlapping notches are not significantly different between pairs (p>0.05).*

Table S7. *Significant differences (p values) between means of air temperatures with WTD bins (Wilcoxon Rank Sum test accommodating non-normal distribution and unequal sample size)*

WTD bin	[0,0.1]	[0.1,0.2]	[0.2,0.3]	[0.3,0.4]	[0.4,0.5]
[0.1,0.2]	< 2e-16	--			
[0.2,0.3]	< 2e-16	< 2e-16	--		
[0.3,0.4]	< 2e-16	< 2e-16	3.40E-05	--	
[0.4,0.5]	< 2e-16	< 2e-16	< 2e-16	2.40E-06	--
[0.5,0.6]	< 2e-16	5.00E-12	0.0805	0.9286	0.0048

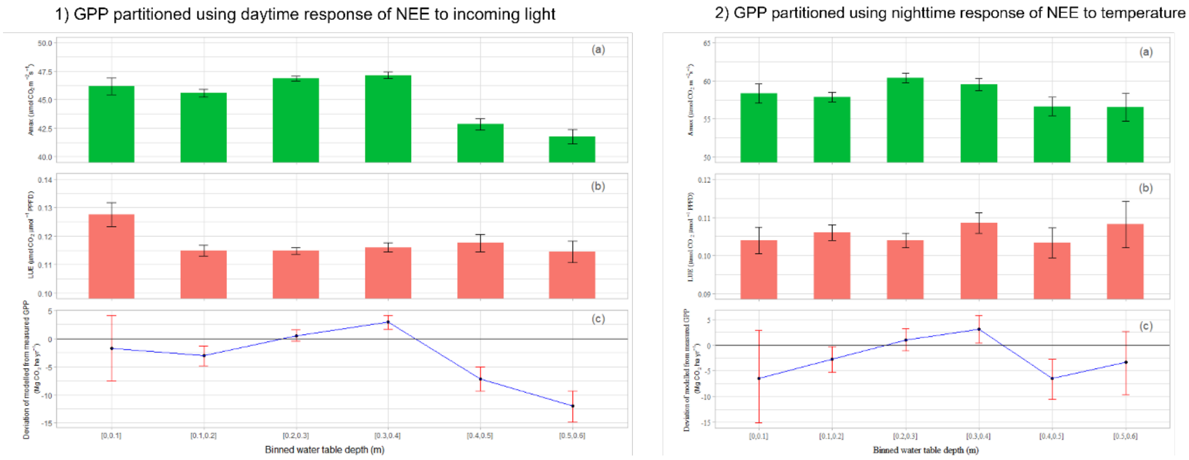

Figure S7. *Modelled estimates of GPP within WTD bins, compared between partitioning methods to establish initial GPP dataset. Plot 1 (left) shows GPP initially derived from response of daytime NEE to incoming light while plot 2 (right) shows GPP initially derived as the residual of Reco estimated from the response of nighttime NEE to temperature (as in main text, Fig. 5).*

References

MONTEITH, J. (1965) Evaporation and environment. In Fogg, G. E. (Ed.), The state and movement of water in living organisms (pp.205-234). 19th *Symp. Soc. Exp. Biol.*, Cambridge University Press, Cambridge

MONTEITH, J, UNSWORTH M. (2008). *Principles of Environmental Physics*. 3rd ed. Academic Press; 2008.

KNAUER, J., EL-MADANY, T. S., ZAEHLE, S. & MIGLIAVACCA, M. 2018. Bigleaf—An R package for the calculation of physical and physiological ecosystem properties from eddy covariance data. *PLoS One,* 13**,** e0201114.

SONNTAG D. 1990: Important new values of the physical constants of 1986, vapor pressure formulations based on the ITS-90 and psychrometric formulae. Zeitschrift fuer Meteorologie 70, 340-344

THOM, A. 1972. Momentum, mass and heat exchange of vegetation. *Quarterly Journal of the Royal Meteorological Society,* 98**,** 124-134.